IMPROVED CANOPY REFLECTANCE MODELING AND SCENE INFERENCE THROUGH IMPROVED UNDERSTANDING OF SCENE PATTERN

Janet Franklin (*Student Researcher*)

David Simonett (*Principal Investigator*)

Department of Geography,
University of California,
Santa Barbara, CA, 93106.

FINAL REPORT

NASA Training Grant NGT 05-010-804

January 31, 1988

PREFACE

We have used a geometric/optical tree canopy reflectance model to study the form and structure of savanna woodland in West Africa. The invertible Li-Strahler model was tested for its ability to estimate tree size and density (woody vegetation amount) from remotely sensed data in areas of sparse woodland.

The following report summarizes the research supported primarily by NASA under Training Grant NGT 05-010-804, and Grant NAGW-788, and comprises the Final Report for the Training Grant. The text that forms the body of this report has been submitted for publication, with NASA's support appropriately acknowledged, to a refereed journal (*IEEE Transactions on Geoscience and Remote Sensing*), with Janet Franklin, and Alan Strahler as authors. This text will also comprise the central chapter of the dissertation submitted by Janet Franklin to the Department of Geography, University of California at Santa Barbara, towards completion of her doctorate.

In addition to the testing of the canopy model, several supporting research tasks were undertaken in the course of the project that involved collaboration with other researchers. While they were not directly a part of the research presented in this report, Janet Franklin's participation in them was at least partially supported by the Training Grant. We anticipate that several research papers will result from those collaborations that are still in progress. We have included abstracts of those tasks in the Appendix. When the tasks are completed and manuscripts are produced, they will acknowledge the support of the NASA Training Grant, and copies will be forwarded to NASA.

INVERTIBLE CANOPY REFLECTANCE MODELING OF VEGETATION STRUCTURE IN SEMIARID WOODLAND

ABSTRACT

The Li-Strahler canopy reflectance model, driven by Landsat Thematic Mapper (TM) data, provided regional estimates of tree size and density within twenty percent of sampled values in two bioclimatic zones in West Africa. This model exploits tree geometry in an inversion technique to predict average tree size and density from reflectance data using a few simple parameters measured in the field (spatial pattern, shape, and size distribution of trees) and in the imagery (spectral signatures of scene components). Trees are treated as simply shaped objects, and multispectral reflectance of a pixel is assumed to be related only to the proportions of tree crown, shadow, and understory in the pixel. These, in turn, are a direct function of the number and size of trees, the solar illumination angle, and the spectral signatures of crown, shadow and understory. Given the variance in reflectance from pixel to pixel within a homogeneous area of woodland, caused by the variation in the number and size of trees, the model can be inverted to give estimates of average tree size and density. Because the inversion is sensitive to correct determination of component signatures, which is a difficult procedure at best, predictions of size and spacing are not very accurate within small (e. g. 10-100 ha) areas. However, individual errors cancel when larger regions are considered, and the procedure may predict size and density of trees over large areas of open woodland with good accuracy.

I. INTRODUCTION

REMOTELY sensed data are commonly used to produce thematic land-cover maps, but also can provide quantitative information on biophysical variables, such as vegetation structure, amount, productivity, (reviewed in [1] and [2]), photosynthesis, and transpiration [3] [4]. These biophysical characteristics of vegetation and their spatial and temporal distribution are critical inputs to ecological models that describe the interaction between the land surface and climate, energy balance, and hydrologic and biogeochemical cycles [5] [6] [7] [8] [9] [10] [11]. Remote sensing provides the only tool that can measure these variables for large areas [12] [13] [14]. In this paper we use a canopy reflectance model and multispectral satellite data to estimate canopy structure in sparse woodland, a vegetation type of great spatial extent and importance.

A family of mathematical models of the reflectance of a plant canopy composed of discontinuous woody cover allows the direct estimation of plant size and density from remotely sensed reflectance data [15]. These Li-Strahler models are geometric in character, treating trees (plants) as solid, discrete, three-dimensional objects on a contrasting background. They use geometric optics to estimate the proportion of each pixel in tree canopy,

shadow, and background. In the simplest model, tree density is assumed to be sufficiently low that the overlapping of trees and shadows may be ignored. Using this simple model, Li and Strahler [15] predicted tree size and density from Landsat MSS data within ten percent of actual values for sparse pine forest in northern California.

We have extended this model and tested it using Landsat Thematic Mapper (TM) data in a different environment where the basic assumptions of the model hold, but the parameters must be modified. The model was tested in sparse woodland and wooded grassland in the Sahelian and Sudanian bioclimatic zones in West Africa.

II. BACKGROUND

In plant canopy reflectance modeling, radiative transfer theory and geometric optics are used to predict the reflectance of a plant canopy as a function of the biophysical properties of the canopy elements, such as the size, shape, spatial distribution and optical properties of plants or plant parts. If a reflectance model can be mathematically inverted, the biophysical properties of the plant stand can be inferred from spectral reflectance measurements. The simple Li-Strahler model describes reflectance as a function of vegetation structure for a canopy composed of large woody plants distributed at low density on the landscape. The model represents an early formulation of a general modeling approach which explicitly treats the interaction of three-dimensional illuminated discrete objects with the spatial sampling interval imposed by a digital image [16] [17] [18] [19] [20] [21] [22]. In the simple model it is assumed that the canopy is imaged by a multispectral scanner with pixel size several times larger than tree size, but with resolution fine enough that the sampling unit interacts with the size and placement of the trees. Thus, the model predicts variance as well as average reflectance. It uses covariance statistics from estimated mixtures of scene components across pixels for inversion to predict average tree size and density in a stand. While other canopy models are invertible, most predict the bidirectional reflectance distribution function (BRDF) of a canopy, and in inversion use field or aircraft radiometric measurements from varying look angles to predict some property of the vegetation, such as Leaf Area Index (LAI) [23]

[24] [25] [26] [27], or leaf reflectance [28]. The Li-Strahler model is different from these other models in that it explicitly considers discretely distributed trees.

A. Formulation of the Canopy Model

The simple Li-Strahler model is discussed in detail elsewhere [15] [29] and will be reviewed in this section for clarity. The only modification to the simple model is the change in the shape parameter. The model assumes that a woodland stand can be modeled geometrically as a group of solid objects (trees) with simple shapes, casting shadows on a contrasting background (understory, grass or soil). Furthermore:

— A tree crown is a simple geometric form. In the sparse woodland, we use an ellipsoid on a stick (Fig. 1) for trees of all sizes.

— Tree counts vary from pixel to pixel as a Poisson function with a fixed density, i. e. the spatial pattern is random at the scale of sensor resolution.

— The size distribution function of trees is known, so that C_{r2}, the coefficient of variation of squared crown radius, can be determined for the stand.

— The tree crown and its associated shadow have spectral signatures that are distinct from that of the background.

The reflectance of a pixel is modeled as a linear combination of the signatures of scene components (illuminated tree crown, illuminated background, shadowed tree, and shadowed background) weighted by their relative areas. Pixels from an area of homogeneous tree cover can be used to estimate average reflectance of a stand of a given density. Interpixel variance exists because the number of trees per pixel and their size distribution vary. In the simple model, we ignore overlapping of trees and shadows, which would also produce pixel-to-pixel variance. Other proportion estimation models similarly predict cover as a function of brightness in canopies with incomplete cover [30] [31] [32] [33] [34] [35]. This effect has been modelled by Otterman [36] [37]. However, the Li-Strahler model solves for tree size and density using the distribution functions and statistical independence of these two parameters.

1) Model Parameters: The variables describing the stand are:

A Area of a pixel.

n Number of trees in a pixel.

N Average density of trees per m^2 in a stand ($= \bar{n}/A$).

r^2 Squared crown radius of tree.

R^2 Average r^2 for a pixel.

$\mathbf{R}^2$ Average R^2 for all pixels in a stand.

C_{r^2} Coefficient of variation of squared crown radius determined for stand.

m $= N\,\mathbf{R}^2$.

Note that since $\pi\mathbf{R}^2$ is the average area of a crown, $m\pi$ is the proportion of woody cover in the stand.

As a three dimensional object, the ellipsoid on a stick casts a shadow on the background. To quantify the area of canopy and shadow, a geometric factor, Γ, is used. Γ is defined such that $m\Gamma$ is the proportion of a pixel covered by tree crown and shadow (i. e. the tree cover adjusted to include shadowing). Based on the geometry of an ellipsoid illuminated at solar zenith angle θ (Fig. 1),

$$\Gamma = \pi + \frac{\pi}{\cos\theta'} - A_0$$

where

$$A_0 = \begin{cases} 0\,, & \text{if } (b+h)\tan\theta > r\left[1+\dfrac{1}{\cos\theta'}\right], \\ r^2\left[\beta - \tfrac{1}{2}\sin 2\beta\right]\left[1+\dfrac{1}{\cos\theta'}\right] & \text{else} \end{cases}$$

and

$$\beta = \cos^{-1}\left[\left[1+\frac{h}{b}\right]\left[\frac{1-\cos\theta'}{\sin\theta'}\right]\right],$$

and

$$\theta' = \tan^{-1}\left[\frac{\tan\theta}{(r/b)}\right].$$

If A_g, A_c, A_z, and A_t are the areas of sunlit background and crown, and shadowed background and crown within the pixel, then

$$A_c + A_t + A_z = m\Gamma$$

and

$$A_g = 1 - m\Gamma.$$

The signature of pixel i in band j, S_{ij}, is then modeled as

$$S_{ij} = (A_g \cdot G_j) + (A_c \cdot C_j) + (A_z \cdot Z_j) + (A_t \cdot T_j) \qquad (1)$$

where G, C, Z and T are the reflectance signatures for a unit area of sunlit background and crown, and shadowed background and crown, respectively. Equation (1) can be written

$$S_{ij} = A_g \cdot G_j + (1-A_g) \cdot X_0$$

where X_0 is the average reflectance of a tree and its associated shadow.

Fig. 2 (modified from [15]) shows an idealized plot of the four spectral components on greenness (i. e. infrared to red contrast) and brightness spectral axes. A bright soil background (G) has high brightness and low greenness, and sunlit canopy (C) has high greenness and is less bright than the background. Shadowed canopy (T) and background (Z) are less bright and less green. The composite tree signature X_0 falls within the triangle CTZ. When cover is low, the pixel signature S varies along the line GX_0 with distance from G proportional to tree cover (m). However, as cover increases, the proportion of shadowed background decreases and the relative proportion of sunlit crown increases. This occurs because shadows fall on the near-vertical sides of trees instead

of the background, and are thus less visible from nadir. At full canopy closure, only sunlit and shadowed crowns are present. The composite tree signature is then X_∞, which falls on the line TC. As coverage increases, the signature will thus diverge from the line GX_0 toward X_∞, and the simple (linear) model is no longer appropriate.

Substituting the expressions for A_g and $(1 - A_g)$, dropping the subscripts in (1) for convenience, and solving for m we have for each pixel

$$m = \frac{G - S}{\Gamma(G - X_0)} . \tag{2}$$

From (2) we can derive the variance of m:

$$V(m) = \frac{V(S)}{\Gamma[(G - X_0)]^2} . \tag{3}$$

where $V(S)$ is the variance in reflectance for all pixels in the stand.

For multiple spectral bands m should be the same if determined from any band. However, variance in the signatures and stand parameters will cause m to vary, and thus m can be taken as a weighted average or selected as the median value.

2) *Model Sensitivity:* The sensitivity of this model to noise in S and the component signatures, and to errors in estimation of parameters, can be shown by taking the partial derivative of m with respect to these variables.

$$\frac{\partial m}{\partial S} = \frac{-1}{\Gamma(G - X_0)}$$

$$\frac{\partial m}{\partial G} = \frac{S - X_0}{\Gamma(G - X_0)^2} \approx \frac{1}{\Gamma(G - X_0)} \quad \text{(because when cover is low } S \approx G\text{)}$$

$$\frac{\partial m}{\partial X_0} = \frac{G - S}{\Gamma(G - X_0)^2} = \frac{m}{G - X_0}$$

$$\frac{\partial m}{\partial \Gamma} = \frac{S - G}{\Gamma^2(G - X_0)} = \frac{-m}{\Gamma}$$

When the spectral contrast between background and tree is high, sensitivity to noise in S, G and X_0 will be reduced, because $(G - X_0)$ is in the denominator. When density is low (m is small), noise or error in estimating X_0 and Γ are less important than the contrast between tree and background $(G - X_0)$, because m is in the numerator.

3) Inversion of the Model: If size and density are independent, then the expressions for the mean and variance of independent products can be applied ([15] p. 709). If $V(R^2) = V(r^2)/n \approx V(r^2)/N$, then

$$V(m) \approx (N + C_{r2}N + C_{r2})(\mathbf{R}^2)^2 = (M + C_{r2}M + C_{r2}\mathbf{R}^2)\mathbf{R}^2. \tag{4}$$

where M is the average m in the stand. Solving for $\mathbf{R}^2$, we obtain:

$$\mathbf{R}^2 = \frac{[(1 + C_{r2})^2 M^2 + 4V(m)C_{r2}]^{1/2} - (1 + C_{r2})M}{2C_{r2}}. \tag{5}$$

Applying the approximation $\sqrt{1 + x} \approx 1 + x/2$, we obtain:

$$\mathbf{R}^2 \approx \frac{V(m)}{(1 + C_{r2})M}. \tag{6}$$

This should be reasonably accurate if $V(m)$ is fairly large. Finally, substituting (2) and (3), the expressions for mean and variance of m, into (5) or (6), $\mathbf{R}^2$ and N can be found from the reflectance values of the pixels in a stand.

III. Study Sites in Mali

The Li-Strahler model was originally developed and tested for sparse pine woodland in northeastern California. However, there are many other landscapes for which the assumptions of the model hold: *Acacia* and broadleaf savanna or woodland in Africa also consist of trees at low density, with a uniform, contrasting understory of grass or soil at some point in the annual cycle. Further, the plants can be regarded as having simple

shapes, invariant with size, and with little overlap, thus casting shadows that can be predicted from tree geometry and sun angle. Savanna canopies are more translucent than conifers, having lower LAI, and cast weaker shadows. The simple model is still applicable because the components' signatures are calibrated from the imagery, although the contrast between G and X_0 will be reduced in this woodland type.

Woodland and savanna, or wooded grassland, will be defined as the subtropical and tropical vegetation formations where the grass stratum is continuous, trees and shrub cover is greater than five percent and less than eighty percent, where fire occurs, and where the growth is closely associated with alternating wet and dry seasons [38]. We chose to test the model for woodland sites in Africa because of the global extent and importance of this physiognomic type. Woodland and wooded grassland cover ten to twenty percent of the land surface, greater than any other surface cover type (except desert and ice) [39]. Dry woodlands and wooded savanna (with tree cover greater than ten percent) are presently estimated to cover 486.4 million ha or 22.2 percent of the continent of Africa, including 8.6 million ha in Mali [40]. Woodlands are often monospecific (one or two dominant types of trees) or nearly so, of low density, have a uniform herbaceous understory, and occur over extensive areas of flat terrain.

We tested the model in study sites in the Sahelian and Sudanian bioclimatic zones in Mali, West Africa (Fig. 3). The Sahel is usually defined with reference to mean annual isohyets and corresponds to the 200-600 mm annual precipitation zone [41] [42] [43] [44] [45]. The vegetation of the Sahel ranges from an open annual grassland with less than ten percent woody cover in the north to perennial grasses with 25 percent or more tree cover in the south. In the Sahelian zone in northern Mali, four test sites were located in the Gourma region, three from among those being monitored by ILCA/Mali (The International Livestock Centre for Africa) in collaboration with the GIMMS Project (Global Inventory, Monitoring and Modeling System; National Aeronautics and Space Administration, Goddard Space Flight Center) [46] [47] [48] [49]. The fourth site was added in this study. Although tree cover is generally low in the Sahel, woodlands are locally dense in low-lying inundated areas, and all of our sites were located in these dense woodland stands (thirty to sixty percent cover). Three of

these sites are dominated by *Acacia seyal*, one by *Acacia nilotica*.

The Sudanian zone is the region to the south of the Sahel, lying between about 11° and 13° N in West Africa, where the rainfall is 600 to 1000 mm, the rainy season lasts 4 to 5 months, and there is permanent agriculture. The vegetation is a mosaic of open woodland savanna, with trees up to 15 m tall, some closed woodland, and edaphic bush thickets and grasslands [50]. The Sudanian test sites are located within the administrative region of Ségou, Mali. The crop/woodland type of vegetation is formed when crops are grown under a woodland of useful trees that are preserved when land is cleared [51]. Three sites are dominated by *Vitellaria paradoxa* (karité), and three by *Acacia albida*. All sites are located in the house fields, cultivated areas near the village where shrubs and weeds are cleared regularly.

We emphasize that these sites were carefully chosen based on prior field investigations, reconnaissance, and photo interpretation, to be representative homogeneous woodland stands of a certain minimum size and range of cover. In order to apply the model more generally, areas of woodland must first be defined in a segmented or stratified image.

IV. Methods

Tree shape parameters and tree cover, size and density were measured in the field to parameterize and test the model. Sites ranged in size from about 9 to 90 ha (100 to 1000 TM pixels), with most sites about 20 to 40 ha (200 to 500 pixels). This corresponds roughly to the size of the 1 km diameter circular plots used by Hiernaux and Justice [48] in their AVHRR study.

Four to eight fixed-radius plots were located systematically within sites (at regular intervals on a rectangular grid or line) in order to sample all parts of the stand, and not bias the location of the plots. Plot radius was fixed within, but variable among sites, and was established by taking preliminary density measurements and choosing a radius that would include approximately fifty trees per site (see Fig. 4 for an example of plot size). Tree height (H), crown diameter (= $2r$), and height to widest crown diameter were measured for all trees in each plot.

Average h and b (see Fig. 1) were calculated for the site, and were used with the sun angle for the TM scene to calculate Γ from the geometry of an ellipsoid on a stick. The model parameter C_{r2} was calculated from sample data for the sites. Size distribution was examined by inspecting histograms of tree size (expressed both as crown size and height) for all sites. Spatial pattern was established by mapping point patterns of 200-900 trees from low-altitude aerial photographs in sample quadrats within test sites for which there was good photo coverage (sites 2, 15 and 20), and analyzing using quadrat analysis [15] [52] and second-order analysis of inter-tree distances [53].

Observed cover for the sites was estimated from the sample plot data. Independent cover estimates for some of the plots from line transect (from [47] and [49]) and photointerpreted point intercept on a grid (by the authors; see [54] for methods) were also used to test the model. These compared favorably with the field measurements, within the expected range of variance (see [22] Table I).

TM data were used to test this model. Early dry season imagery was chosen to enhance the contrast between trees (still green for most species) and background (a dry herbaceous layer, or bare soil). The TM scene for the Sahelian sites was acquired 9 September 1984 at the end of a very poor rainy season [48] [55], but just after a local rainfall event in the study area [46]. A second Sahelian scene, acquired 7 May 1985 at the end of the dry season, was also used to test the model. The scene for the Sudanian sites dates from 17 November 1984, after the harvest, so the fields beneath the tree canopy have been cleared. The mean and variance of reflectance for all pixels (S and $V(S)$) were computed for each spectral band in the test sites.

The component signatures required by the model are simply the relative brightnesses of the components (background, tree and shadows) compared to the mean brightness of the stand, not the absolute radiance or reflectance. The signatures were established from the satellite data, because it would have been very difficult to calibrate them accurately from field radiometer measurements in a heterogeneous environment, and to project them through a modelled atmosphere. Signatures for background and canopy (G and X_0) were initially computed from small training areas in the image, using aerial photographs as a guide. Areas of no tree cover in or

near sites were used to estimate G, and pixels with high tree cover were used to estimate X_0. Comparable and satisfactory results were obtained by automatically choosing the extreme pixel values from the histogram of the brightness values in the site as the G and X_0 signatures. It was possible to predict G and X_0 using the model in these sites for which N and $\mathbf{R}^2$ were known, and compare predicted values to those observed in training sites or the histograms.

The model was tested by providing the stand parameters (Γ and C_{r2}) and the spectral parameters (G, X_0, S and $V(S)$), predicting $\mathbf{R}^2$ and N for each site, and comparing to actual $\mathbf{R}^2$ and N from field measurements. Observed and predicted values were compared by simple regression. The model was tested for all visible and infrared TM bands (1-5 and 7; see Table I for wavelength bands) and then for a subset of bands, TM 3, 4 and 7. Band 3 was chosen because in our experience red reflectance is strongly related to tree cover [56] [57], Band 4 because of its relationship to green vegetation amount [58], and Band 7 because it had the highest variance in the sites, and has also been shown to be related to tree cover [59]. These bands are from different regions of the spectrum and tend to be uncorrelated. Finally, the model was tested using transformed spectral channels, the NDVI (Normalized Difference Vegetation Index [60] [61]) representing image greenness, and the first principal component representing image brightness.

V. Results

A. Stand Parameters

The tree shape measurements for the sites (height, $\overline{H}$, and crown radius, $\overline{r}$) and the derived model parameters Γ and C_{r2} are shown in Table II. The trees in the Sudanian sites are taller, with relatively narrower crowns, and in the Sahelian sites, the trees are shorter with relatively wider crowns. In site 15 the trees are essentially balls of foliage sitting on the ground, and Γ is smaller than for site 101 because even though the average crown is smaller in 101, it is elevated off the ground and more shadow is visible. The average Γ for the Sahelian sites is 5.1. The Sudanian sites have larger Γ because the TM scene was imaged later in the fall so the solar angle is greater. Average Γ for the Sudanian sites is 7.1.

Tree size distributions for all sample populations were slightly to extremely right-skewed. This concurs with other studies of the West African savanna (summarized in [62]). Log-transforms produced normal-looking distributions. Fig. 5 presents two examples of size parameters (crown area and height) as log-normalized. Thus, if field measurements were not available, the assumption of a lognormal size distribution is valid for these sites, and the formula for C_{r2} for a lognormal distribution could be used. However, for these sites C_{r2} was calculated directly from sample data, and ranges from .26 to .77 (Table II). There is no apparent difference in the C_{r2} values between the two regions; however, the value is sensitive to the presence of a few very large crowns in the sample population (as in sites 2 and 15).

Fig. 6 shows the point locations and results of second order analysis for one of the sites. In all sites there is generally an inhibition distance of five to ten meters, below which the probability of finding two trees is very low, but at relevant sensor resolution (20 to 50 m) a Poisson model is adequate. This is supported by the quadrat analysis (Table III). At larger distances (50 to 100 m) a Poisson model still fits in many of the sites, including the sparser stands (site 2) at densities where the Poisson model broke down in our earlier studies of California pine stands [15].

The actual tree size (expressed as squared crown radius), density, and cover for the sample sites are shown in Table IV. Sahelian sites have small trees at higher density. Sudanian sites have very large trees at low density, and generally lower cover.

In order to compare observed size, density and cover with predicted values obtained by model inversion, estimates of sample variance in these quantities are required. These estimates help to indicate how much of the difference between the predicted and observed values results from sample variance rather than disagreement between model and measurement. For r^2, variance is simply determined using the many individual tree count measurements for all plots taken at a site. However, for N, the sample size within a site was small, ranging from four to eight. To determine whether or not sample variance should be based on within-site measurements, or are sufficiently similar between sites or regions that pooled estimates should be used, we conducted three

analyses of variance (ANOVAs) (Table V). The ANOVAs showed significant difference at region and site levels, indicating that pooling was inappropriate. Accordingly, the standard deviations shown in Table IV are based on within-site measurements.

B. Effect of Model Approximations:

Equation (6) was almost always the best predictor, although in a few cases Equation (5) was better. Therefore, (6) was accepted as being a reasonable approximation ($V(m)$ was fairly large), and in all analyses, the results from this approximation are presented.

C. Early vs. late dry season imagery:

For the Sahelian study region, we hypothesized that the September 1984 image (recorded following a rainfall event) would have a green herbaceous layer of varying density or standing water in sites 15, 20 and 21, causing low separability of component signatures, and that late dry-season (May 1985) imagery would work better in the model. This is true for site 20, the only site for which G_{obs} (brightest pixel in stand) is *darker* than G_{pred} (probably due to herbaceous growth or inundated soil in the site). However, the May 1985 late dry season imagery did not consistently predict cover better than the 1984 imagery for the Sahelian sites (see Fig. 7). It is difficult to discern a pattern with only four points; however, it appears that as long as there is some spectral contrast between background and tree, the model can be inverted. It can be seen in Fig. 8 (shown for 1984 data) that for sites 15 and 101, G and X_0 don't separate well in greenness (NDVI), but the contrast is better in brightness, and the predictions of the model are reasonable.

D. Effect of Stand Parameters:

We used the average values of C_{r2} (.45) and Γ (7.1 for Sudanian scene, 5.1 for Sahelian), and there was no systematic change in the accuracy of predictions. There is little change in the predicted values of R^2 and N, and no systematic error caused by holding the stand variables constant. Predicted cover values only changed by three to four percent, improving or degrading the prediction by only that much (Table VI).

E. Effect of Shape Model:

In order to evaluate the effects of shape on the inversion procedure, we developed an alternative formulation of Γ for the shape of a hemisphere on a stick. At least some of the trees in each plot could be considered to fit this shape reasonably well. To test this change, we calculated Γ for the sites using the hemisphere model to see if it performed better or worse than that of an ellipsoid. There was no consistent difference in the results using the hemisphere shape. As Γ increases, predicted R^2 increases (and predicted N doesn't change), so, as Γ increases results should improve in cases where cover was underestimated, and vice versa. Since there were cases where cover was over- and underestimated, there was no overall improvement in model results (see Table VI).

F. Component Signature Estimation:

Using unadjusted component signatures, density (N) is overestimated and size (R^2) is underestimated for all sites and all bands. This is because the brightest pixel reflectance in the stand (or signatures from training sites) are overestimates of the background signature G. If G is overestimated, the model predicts too many trees, and if N goes up, R^2 must go down, so size is underestimated. When observed and predicted G and X_0 were regressed, the coefficient of determination (r^2) values were very high (.96-.99). The distributions of G_{pred}/G_{obs} and X_{0pred}/X_{0obs} were very peaked (see Fig. 9), so the average (median) values of G_{pred}/G_{obs} and X_{0pred}/X_{0obs} in each region were used to scale G and X_0 (.90 and 1.15 in the Sudanian sites, .98 and 1.05 in the Sahelian sites). Thus, G is slightly darker than the brightest pixel and X_0 slightly brighter than the darkest in all spectral channels including the near-infrared (Band 4), and in composite image brightness (the first principal component of the spectral data). This pattern is reversed in composite image greenness (the NDVI in this analysis). When G and X_0 are adjusted using these simple scaling factors, the results improved, especially for predictions of cover and density. This adjustment was necessary for obtaining reasonable predictions, even though it only changed the signatures by a few DNs ("digital numbers" or brightness levels, quantized to 256 levels for TM data) because of the extreme sensitivity of the model to the component signatures, especially to

the background signature G.

G. Multispectral Predictions

We tested the model for single spectral bands for all sites (each band is assumed to be an independent predictor). When observed and predicted size and density were compared for all sites and all single bands, the results were highly variable. However, the results substantially improved when the median predictions from among the bands was compared to the observed value. The median improved the correlation between observed and predicted values because the scaling of G sometimes caused spurious results for a band. For example, if scaled G (G_{pred}) was closer than S to X_0, the result was a negative R^2 prediction, or an extremely large predicted N. Because the spectral bands are correlated within spectral regions, the results were also calculated for the median prediction from Bands 3, 4, and 7, bands which are not strongly correlated (Fig. 7 and Table VI). Results are slightly better for the six band median. Fig. 7 (e) and (f) also shows that although the variance in observed N and R^2 (estimated from the plot data) is large in some cases, it is not as great in the "variance" in the multispectral predictions (shown as the range of the three-band prediction).

H. Transformed Spectral Channels

Successful inversion of the model requires good spectral separability of G and X_0 (Fig. 2); thus, we explored the use of multiband transforms to define G and X_0. For this analysis, we selected the first principal component of the images as a brightness channel, and used the NDVI as a greenness channel. Although NDVI is not necessarily orthogonal to the first principal component, it is well known to respond to green vegetation in a fashion independent of image brightness. Averaging the predictions of size and density obtained from these two transformed bands did not produce a better result than the median of Bands 3, 4 and 7 (Table VI), but the results are helpful for graphic interpretation because they correspond to the idealized spectral channels used by Li and Strahler in their original formulation of the model. The effect of scaling G is to create a linear relationship between G, S and X_0. Fig. 8 shows the position of G, X_0 and S for the Sahelian sites (15, 20, 21, 101) for both observed and predicted (adjusted) values of G and X_0. Separation between G and X_0 is best for sites

20 and 21, and cover, size and density are predicted more accurately for these sites than for sites 15 and 101 where separation is poorer. The patterns are similar for the Sudanian sites.

I. Regional Estimates

When the observed and predicted tree size and density are averaged for all sites in a region, the results clearly differentiate the two distinctive regions. As Table VII shows, the tree dimensions and distribution are very different in the two regions and the averaged predictions for size and density are very close to the observed averages for the regions. T-tests show that the regions have significantly different average size and density (all at least at the 0.0005 level). Observed and predicted values for each region are not significantly different; however, it should be noted that the sample size for the t-test is small.

VI. Summary and Discussion

The models doesn't predict tree size very well for the ten test sites ($r^2 = .20$). Size is both under- and overestimated. The model predicts density and cover better (r^2 is .62 to .78) in these test sites, where cover ranges from approximately ten to forty percent. It is a reasonable assumption that $V(m)$ (variance in cover among pixels) is large at this sampling scale (30 m TM pixels), and Equation (6) can be used to approximate R^2 for these samples (100-1000 pixels).

The results support our prediction that the model is sensitive to the choice of the G signature and to the separability of G and X_0. When G is overestimated, tree size is systematically underestimated, and density overestimated. Scaling G dramatically improved results. Sites and spectral bands with good separability between G and X_0 generally showed better predictions (sites 1, 20, 21, Bands 3, 5, 7), although there were exceptions. Also in support of our predictions for these sites with low cover (small m), the model is not sensitive to variance or error in estimating tree shape and size parameters (Γ and C_{r2}). Using a different shape model that slightly changed Γ, or using standardized Γ and C_{r2} had very little effect on the overall results.

Best results were obtained by using all spectral channels for the predictions, and selecting the median value from among them. This is because scaling the component signatures can cause spurious results for an

individual band. The best results come from selecting the median predictions from all six visible and infrared TM bands, even though some spectral bands are strongly correlated, and the predictions are therefore not independent. Reasonable predictions of tree size and density were also obtained using three largely uncorrelated bands (3, 4 and 7). Neither parameter was systematically over- or underestimated for the sites.

The sites that were not predicted well are helpful in illustrating the limits of the simple model. Cover is underestimated in site 20, which has the highest cover value. As cover increases, trees and shadows do, in fact, overlap. X_0 will approach X_∞ as shown in Fig. 2. Therefore, our estimate of X_0 is too dark, and for a given brightness, tree cover will be underestimated. Either tree size is underestimated when variance is low, or density is underestimated when variance is higher. However, in this site the actual cover may also be overestimated by our plot data (see Fig. 7 (d) and Table IV).

For several of the sites (2, 4, 5, 7), tree density is as low as one to three trees per pixel. In this case, the predictions of the model will be strongly influenced by variations in the background (G). This will contribute to errors in the prediction of both N and $\mathbf{R}^2$. Also, X_0 will be incorrectly estimated at low density, causing errors in the prediction of $\mathbf{R}^2$. This can be seen in site 7. The darkest pixel in the stand doesn't represent X_0 because it contains background. Therefore X_0 is too bright and R^2 is overestimated. If X_0 is assigned a lower brightness, closer to the values for the other *Vitellaria paradoxa* sites ($X_0 = .98\,X_0$), the predicted value is much closer to observed (see Fig. 7 (c)).

In site 2, density is overestimated and cover underestimated. This may be because scaled G is still brighter than the actual background signature, although when inspecting the imagery for the stand, there are not any anomalously bright pixels included in the training data. However, our photointerpreted cover for the stand is much greater than is calculated from the plot data, and closer to the value predicted from the model. In this case the observed values for tree size and density may be low, due to sample variance or errors in the field measurements.

We conclude that at this scale, in small sites on the order of 0.5 km^2, variations in the understory signature and other stand parameters cause site-specific predictions, particularly of tree size, to be poor. However, when predictions are averaged within the Sudanian and Sahelian regions, regional differences in the structure of these woodland types are accurately detected and quantified by the inversion procedure.

Therefore, this procedure could be used most effectively as part of a multistage inventory to estimate the average size and density of woody plants directly over large areas in woodlands ranging from ten to forty percent cover. In an automated procedure, G and X_0 could be selected from the histograms for twenty or thirty sites in a stratified region. C_{r2} and Γ can be chosen *a priori* for a vegetation type. We would expect a good prediction of tree size and density for a stratum within a region based on the average from these sites. We feel that the model could be inverted using Landsat MSS data in this landscape because stands are sufficiently large that even at 80 m resolution there are enough pixels (100 or more) to estimate variance.

Because size and spacing are often related to leaf and woody biomass, this technique could also provide woodland biomass estimates over large areas [63]. Besides their obvious relationship to standing biomass, important enough in itself, height and spacing could be used to determine surface roughness and other parameters important to land-surface climatological models [11]. Also, regional-scale ecological models of ecosystem photosynthetic production and biogeochemical cycling may require input parameters of vegetation structure of the type obtainable through our inversion procedure [4] [64]. This is especially true in open woodland where tree canopy is not homogeneous, and its interaction with radiation and the atmosphere near the ground cannot be approximated by homogeneous plane-parallel models.

Finally, the inversion procedure may help monitor desertification — the spread of desert-like conditions into arid and semi-arid lands, such as the Sahel, caused by drought and overexploitation of vegetation and soil in the region [65]. In general, drought reduces density by killing individual trees (observed by Poupon [66]), while over-use of trees (coppicing and woodcutting for fuel and fodder) reduces crown area, while number of individuals may actually increase [67]. These two phenomenon could be distinguish in a regional context using the

inversion procedure, which could be applied to historical Landsat data to examine changes in the recent past.

ACKNOWLEDGEMENTS

We are indebted to Roy Cole, Mohamed Idriss Cissé, Dramane Dembélé, Dramane Diarra, Lassine Diarra, Pierre Hiernaux, Aboubakrine Mahamar, Issouf Maiga, Moussa Traoré and many others who acted as advisors, colleagues, guides, assistants and hosts in Mali. The fieldwork in the Region of Ségou was conducted with authorization of the National Ministry of Education, Mali. The fieldwork in the Gourma was conducted with the permission and support of ILCA/Mali, Dr. Abdelkader Diallo, Director. This project would not have been possible without the support of Chris Justice and the GIMMS project at NASA Goddard Space Flight Center. We would like to thank Jeff Dozier, Joel Michaelsen, David Simonett and Li Xiaowen for their suggestions, comments, and help.

REFERENCES

[1] Ajtay, G. L, Ketner, P., and Duvigneaud, P., "Terrestrial primary production and phytomass," in *The Global Carbon Cycle*, ed. B. Bolin, E.T. Degens, S. Kempe and P. Ketner, pp. 129-181, SCOPE 13, John Wiley and Sons, New York, 1979.

[2] Aubréville, A., *Climats, Foret et Desertification de l'Afrique Tropicale*, 351 pp., Soc. Ed. Geogr. Marit-et Cd., Paris, 1949.

[3] Bille, J. C., "Mesure de la production primaire appetée des ligneux," in *Browse in Africa, the Current State of Knowledge*, ed. H. N. Le Houerou, pp. 183-193, International Livestock Centre for Africa, Addis Ababa, Ethiopia, 1980.

[4] Botkin, D. B., Estes, J. E., MacDonald, R. M., and Wilson, M. V., "Studying the Earth's vegetation from space," *BioScience*, vol. 34, pp. 508-514, 1984.

[5] Boudet, G., *Rapport sur la Situation Pastorale dans les Pays du Sahel*, 45 pp., UN FAO/EMASAR, IEMVT, Rome, 1975.

[6] Bourlière, F. and Hadley, M., "Present-day Savannas: An Overview," in *Tropical Savannas*, ed. F. Bourlière, pp. 1-18, Elsevier Scientific Publishing Company, Amsterdam, 1983.

[7] Breman, H. and Witt, C. T. de, "Rangeland productivity and exploitation in the Sahel," *Science*, vol. 221, pp. 1341-1347, 1983.

[8] Brown-Frederickson, M. E., Vogler, V. J., and Adams, J. D., "Estimation of percentage vegetation for range management using Landsat MSS images," *Proceedings of the RNRF Symposium on the Application of Remote Sensing to Resource Management*, Seattle, Washington, 1983.

[9] Curran, P., "Multispectral remote sensing of vegetation amount," *Progress in Physical Geography*, vol. 4, pp. 315-341, 1980.

[10] Diarra, L. and Hiernaux, P., "Evolution de la végétation sahélienne après la sécheresse bilan du suivi des sites du Gourma en 1986," Programme des Zones Aride et Semi-aride, Document du Programme, Centre International pour l'Elevage en Afrique (CIPEA), Bamako, Mali, 1987.

[11] Franklin, J., "Thematic Mapper analysis of coniferous forest structure and composition," *International Journal of Remote Sensing*, vol. 7, pp. 1287-1301, 1986.

[12] Franklin, J. and Hiernaux, P. H. Y., "Estimating leaf and wood biomass in Sahelian and Sudanian woodlands using a remote sensing model," *in preparation*, 1988.

[13] Franklin, J., Michaelsen, J., and Strahler, A. H., "Spatial analysis of density dependent pattern in coniferous forest stands," *Vegetatio*, vol. 64, pp. 29-36, 1985.

[14] Getis, A., "Interaction modeling using second-order analysis," *Environment and Planning A*, vol. 16, pp. 173-183, 1984.

[15] Goel, N. S. and Deering, D. D., "Evaluation of a canopy reflectance model for LAI estimation through its inversion," *IEEE Transactions on Geoscience and Remote Sensing*, vol. GE-23, pp. 674-684, 1985.

[16] Goel, N. S. and Strebel, D. E., "Inversion of vegetation canopy reflectance models for estimating agronomic variables. I. Problem definition and initial results using the Suits model," *Remote Sensing of*

Environment, vol. 13, pp. 487-507, 1983.

[17] Goel, N. S., Strebel, D. E., and Thompson, R. L., "Inversion of vegetation canopy reflectance for estimating agronomic variables. II. Use of angle transforms and error analysis as illustrated by the Suits model," *Remote Sensing of Environment*, vol. 15, pp. 77-101, 1984.

[18] Goel, N. S. and Thompson, R. L., "Inversion of vegetation canopy reflectance for estimating agronomic variables. III. Estimation using only canopy reflectance data as illustrated by the Suits model," *Remote Sensing of Environment*, vol. 15, pp. 223-236, 1984.

[19] Goel, N. S. and Thompson, R. L., "Inversion of vegetation canopy reflectance for estimating agronomic variables. IV. Total inversion of the SAIL model," *Remote Sensing of Environment*, vol. 15, pp. 237-253, 1984.

[20] Graetz, R. D. and Gentle, M. R., "The relationships between reflectance in the Landsat wavebands and the composition of an Australian semi-arid shrub rangeland," *Photogrammetric Engineering and Remote Sensing*, vol. 48, pp. 1721-1730, 1982.

[21] Heimes, F. J. and Smith, J. A., "Spectral variability in mountain terrain," Final Report, Rocky Mountain Forest and Range Experiment Station U. S. Forest Service Cooperative Agreement 16-625-CA, 1977.

[22] Hiernaux, P., "L'inventaire du potentiel fourrager des arbres et arbustes d'une region du Sahel Malien. Méthods et premiers résultats," in *Browse in Africa, the Current State of Knowledge*, ed. H. N. Le Houerou, pp. 195-201, International Livestock Centre for Africa, Addis Ababa, Ethiopia, 1980.

[23] Hiernaux, P., Cissé, M. I., and Diarra, L., "Bilan d'une saison d'es pluies 1984 très déficitaire dans la Gourma (Sahel Malien). Première campagne de suivi et télédetection expérimentale, Annexe: Fiches descriptives des sites," Programme des Zones Aride et Semi-aride, Document du Programme, Centre International pour l'Elevage en Afrique (CIPEA), Bamako, Mali, 1984.

[24] Hiernaux, P. and Diarra, L., "Pour une technique de télédetection appliquée au sui de l'evolution de la végétations sahélienne," Programme des Zones Aride et Semi-aride, Document du Programme, Centre

International pour l'Elevage en Afrique (CIPEA), Bamako, Mali, 1986.

[25] Hiernaux, P. H. Y. and Justice, C. O., "Suivi du développement végétal au cours de l'été 1984 dans le Sahel Malien," *International Journal of Remote Sensing*, vol. 7, pp. 1515-1531, 1986.

[26] Holben, B. N., Tucker, C. J., and Fan, C. J., "Spectral assessment of soybean leaf area and leaf biomass," *Photogrammetric Engineering and Remote Sensing*, vol. 46, pp. 651-656, 1980.

[27] Horler, D. N. H. and Ahern, F. J., "Forestry information content of Thematic Mapper data," *International Journal of Remote Sensing*, vol. 7, pp. 405-428, 1986.

[28] Houghton, R. A., Hobbie, J. E., Melillo, J. M., Moore, B., Peterson, B. J., Shaver, G. R., and Woodwell, G. M., "Changes in the carbon content of the terrestrial biota and soils between 1860 and 1980: A net release of carbon to the atmosphere," *Ecological Monographs*, vol. 53, pp. 235-262, 1983.

[29] Jackson, R. D., Reginato, R. J., Jr., P. J. Pinter, and Idso, S. B., "Plant canopy information extraction from composite scene reflectance of row crops," *Applied Optics*, vol. 18, pp. 3775-3782, 1979.

[30] Jensen, J., "Biophysical remote sensing," *Annals of the Association of American Geographers*, vol. 73, pp. 111-132, 1983.

[31] Jupp, D. L. B., Strahler, A. H., and Woodcock, C. E., "Autocorrelation and regularization in digital images I. Basic theory," *IEEE Transactions on Geoscience and Remote Sensing*, 1987. Submitted.

[32] Jupp, D. L. B., Strahler, A. H., and Woodcock, C. E., "Autocorrelation and regularization in digital images II. Simple image models," *IEEE Transactions on Geoscience and Remote Sensing*, 1987. Submitted.

[33] Lanley, J. P. and Clement, J., "Tropical Forest Resources Assessment Project (in the framework of GEMS - Global Environmental Monitoring System)," in *Forest Resources of Tropical Africa, Part 1-Regional Synthesis*, UN FAO/UNEP (United Nations Food and Agricultural Organization/ United Nations Environmental Programme), Rome, 1982.

[34] Le Houerou, H. N., "The rangelands of the Sahel," *Journal of Rangeland Management*, vol. 33, pp. 41-46, 1980.

[35] Li, X., "Geometric-optical modeling of a conifer forest canopy," Ph.D. Dissertation, Department of Geography, University of California, Santa Barbara, CA, 1983.

[36] Li, X. and Strahler, A. H., "Geometric-optical modeling of a conifer forest canopy," *IEEE Transactions on Geoscience and Remote Sensing*, vol. GE-23, pp. 705-721, 1985.

[37] Li, X. and Strahler, A. H., "Geometrical-optical bidirectional reflectance modeling of a coniferous forest canopy," *IEEE Transactions on Geoscience and Remote Sensing*, vol. GE-24, pp. 906-919, 1986.

[38] Logan, T. L. and Strahler, A. H., "Optimal Landsat transforms for forest applications," *Proceedings of the Sixteenth International Symposium on Remote Sensing of Environment*, pp. 455-468, Ann Arbor, Michigan, 1982.

[39] Mabbutt, J. A., "Perspectives on desertification," *Economic Geography*, vol. 53, pp. 429-432, 1977.

[40] Mintz, Y., *The Global Climate*, Bracknell, United Kingdom, 1984.

[41] NASA, "Land-Related Global Habitability Science Issues," NASA Technical Memorandum 85841, National Aeronautics and Space Administration, July, 1983.

[42] National Academy of Sciences (NAS) Committee of Planetary Biology, "Remote Sensing of the Biosphere," Space Sciences Board Commission on Physical Sciences, Mathematics and Resources, National Research Council, National Academy Press, Washington, D.C., 1986.

[43] Nielsen, M., *Introduction to the Flowering Plants of West Africa*, University of London Press, London, 1965.

[44] Otterman, J., "Albedo of a forest modeled as a plane with dense vertical protrusions," *Journal of Climate and Applied Meteorology*, vol. 22, pp. 297-307, 1984.

[45] Otterman, J., "Bidirectional and hemispherical reflectivities of a bright soil plane and a sparse dark canopy," *International Journal of Remote Sensing*, vol. 6, pp. 897-902, 1985.

[46] Otterman, J., Strebel, D. F., and Ranson, K. J., "Inferring spectral reflectances of plant elements by simple inversion of bidirectional reflectance measurements," *Remote Sensing of Environment*, vol. 21, pp. 215-228, 1987.

[47] Pech, R. P., Graetz, R. D., and Davis, A. W., "Reflectance modelling and the derivation of vegetation indices for an Australian semi-arid shrubland," *International Journal of Remote Sensing*, vol. 7, pp. 389-403, 1986.

[48] Penning de Vries, F. W. T. and Djitéye, M. A., *La Productivité des Paturâges Sahéliens: Une Etude de l'Exploitation de cette Ressource Naturelle*, Centre for Agricultural Publishing and Documentation, Wageningen, Holland, 1982.

[49] Poupon, H., "Production de matiere seche d'*Acacia senegal* (L.) Willd. dans une savane sahelienne au Senegal," *Geo-Eco-Trop*, vol. 3, pp. 209-228, 1977.

[50] Rasool, S. I., "On dynamics of desert and climate," in *The Global Climate*, ed. J. T. Houghton, pp. 107-120, Cambridge University Press, Cambridge, 1983.

[51] Richardson, A. J., Weigand, E. C., Gausman, H., Cuellar, J., and Gerberman, A., "Plant, soil and shadow reflectance components of row crops," *Photogrammetric Engineering and Remote Sensing*, vol. 41, pp. 1401-1407, 1975.

[52] Robertson, G. P. and Rosswall, T., "Nitrogen in West Africa: The regional cycle," *Ecological Monographs*, vol. 56, pp. 43-57, 1986.

[53] Rosswall, T. H., "The biogeochemical nitrogen cycle," in *Some Perspectives on the Major Biogeochemical Cycles*, ed. G. E. Likens, pp. 25-49, John Wiley and Sons, Chichester, 1981.

[54] Schnell, R., *Introduction á la Phytogéographie des Pays Tropicaux: 3. La Flore et la Végétation de l'Afrique Tropicale*, Gauthiers-Villars, Paris, 1977.

[55] Sellers, P. J., "Canopy reflectance, photosynthesis and transpiration," *International Journal of Remote Sensing*, vol. 6, pp. 1335-1372, 1985.

[56] Sellers, P. J., "Canopy reflectance, photosynthesis, and transpiration. II. The role of biophysics in the linearity of their interdependence," *Remote Sensing of Environment*, vol. 21, pp. 143-183, 1987.

[57] Sellers, P. J., Mintz, Y., Sud, Y. C., and Dalcher, A., "A simple biosphere model (SiB) for use within general circulation models," *Journal of the Atmospheric Sciences*, vol. 43, pp. 505-531, 1986.

[58] Strahler, A. H., Woodcock, C. E., and Smith, J., "On the nature of models in remote sensing," *Remote Sensing of Environment*, vol. 20, pp. 121-139, 1986.

[59] Townshend, J. R. G. and Justice, C. O., "Analysis of the dynamics of African vegetation using the normalized difference vegetation index," *International Journal of Remote Sensing*, vol. 7, pp. 1435-1445, 1986.

[60] Tucker, C. J., "Red and photographic infrared linear combinations for monitoring vegetation," *Remote Sensing of Environment*, vol. 8, pp. 127-150, 1979.

[61] Tucker, C. J., Fung, I. Y., Keeling, C. D., and Gammon, R. H., "Relationship between atmospheric CO_2 variations and a satellite-derived vegetation index," *Nature*, vol. 319, pp. 195-198, 1986.

[62] Tucker, C. J., Holben, B. N., Elgin, J. H., and McMurtrey, J. E., "Remote sensing of total dry-matter accumulation in winter wheat," *Remote Sensing of Environment*, vol. 11, pp. 171-189, 1981.

[63] Warren, P. L. and Dunford, C., "Vegetation sampling with large scale aerial photography," *Remote Sensing Newsletter*, vol. 83, pp. 1-6, University of Arizona, 1983.

[64] Woodcock, C. E. and Strahler, A. H., "The factor of scale in remote sensing," *Remote Sensing of Environment*, vol. 21, pp. 311-332, 1987.

[65] Woodcock, C. E., Strahler, A. H., and Jupp, D. L. B., "The use of variograms in remote sensing I: Scene models and simulated images," *Remote Sensing of Environment*, 1987. Submitted.

[66] Woodcock, C. E., Strahler, A. H., and Jupp, D. L. B., "The use of variograms in remote sensing II: Real digital images," *Remote Sensing of Environment*, 1987. Submitted.

[67] Woodwell, G. M., *The Role of Terrestrial Vegetation in the Global Carbon Cycle*, 247 pp., Wiley, New York, 1984.

Table I

TM SPECTRAL BANDS

TM band	Wavelength (μm)
1	0.45-0.52
2	0.52-0.60
3	0.63-0.69
4	0.76-0.90
5	1.55-1.75
7	2.08-2.35

Table II

TREE SHAPE MEASUREMENTS FOR STUDY SITES

Site	Species	n	Height (m)		Crown Radius (m)		Γ	$C_{r,z}$
			mean	σ	mean	σ		
SUDANIAN SITES								
1	*Vitellaria paradoxa*	35	8.35	2.44	3.67	1.19	7.00	.5164
2	*Vitellaria paradoxa*	50	8.61	2.94	4.13	1.60	6.67	.7780
3	*Acacia albida*	32	11.07	1.96	4.15	1.02	7.28	.2612
4	*Acacia albida*	63	13.17	3.01	5.57	2.06	7.10	.5682
5	*Acacia albida*	60	11.58	2.58	4.91	1.72	7.07	.5616
7	*Vitellaria paradoxa*	50	12.60	2.71	4.72	1.36	7.55	.2969
SAHELIAN SITES								
15	*Acacia nilotica*	56	5.64	1.59	3.56	1.25	4.72	.6816
20	*Acacia seyal*	87	5.27	1.66	3.06	1.08	5.00	.4385
21	*Acacia seyal*	75	4.88	1.53	2.50	0.88	5.30	.5151
101	*Acacia seyal*	105	5.02	1.16	2.45	0.90	5.30	.5797

Table III

QUADRAT ANALYSIS: FIT TO POISSON DISTRIBUTION

Quadrat Size	*n* quadrats	*n* points	mean	χ^2	df
Site 15 (*Acacia nilotica*)					
10	784	587	0.7	4.7	3
20	196	587	3.0	4.7	9
25	121	567	4.7	8.0	12
30	81	547	6.8	3.1	13
35	64	587	9.2	9.1	18
40	49	587	12.0	20.9	24
50	25	466	18.6	~10	27
Site 20 (*Acacia seyal*)					
20	182	838	4.6	10.0	10
25	121	877	7.2	24.8	18
30	81	850	10.5	25.9	19
35	56	780	13.9	~15	28
40	42	757	18.0	~51*	30
Site 2 (*Vitellaria paradoxa*)					
10	625	223	0.36	3.1	0
20	144	212	1.47	0.3	4
30	64	213	3.3	3.9	7
40	36	213	5.9	5.8	14
50	25	223	8.9	6.4	17
60	16	213	13.1	11.3	26

* significantly different at .05 level

Table IV

ACTUAL TREE SIZE, DENSITY, AND COVER

Site	(Crown radius)^2 (m^2)			Density (ha^{-1})			Cover (%)	
	mean	σ	*n*	mean	σ	*n*	sampled	photo
SUDANIAN SITES								
1	14.85	10.67	35	45.74	13.84	4	22	
2	19.58	17.27	50	30.36	6.65	6	19	27
3	18.25	9.33	32	35.72	7.44	4	21	
4	35.18	26.52	63	21.40	12.23	8	24	
5	27.02	20.25	60	12.74	8.37	6	11	
7	24.05	13.11	50	10.61	3.08	6	08	
SAHELIAN SITES								
15	14.21	11.73	56	71.30	40.53	4	32	23
20	10.53	6.97	87	168.07	24.63	3	56	39
21	7.03	5.04	75	149.21	26.29	4	33	44
101	6.82	5.19	105	133.69	154.55	4	29	

Table V

ANOVA OF DENSITY IN SAMPLE SITES

Source of Variation	*F*	*p*
Regions vs. plots within regions	1357.51	0.0000
Sudanian Sites, sites vs. plots within sites	61.82	0.0000
Sahelian Sites, sites vs. plots within sites	4.51	0.02
Sahelian Sites, without site 101	61.82	0.0000

Table VI

SUMMARY OF MODEL RESULTS
REGRESSION, OBSERVED VS. PREDICTED STAND PARAMETERS

Trial	a	b	r^2
COVER			
Six Bands Median	.674	+.036	.74
Bands 3, 4, 7 Median	.922	+.094	.62
Standard Γ and $C_{r,2}$	.038	+.682	.72
Hemisphere shape model	.039	+.652	.76
TREE SIZE (R^2)			
Six Bands Median	.586	+8.352	.28
Bands 3, 4, 7 Median	.756	+7.449	.16
Standard Γ and $C_{r,2}$	.348	+6.511	.18
Hemisphere shape model	.399	+5.207	.18
Brightness and NDVI	.270	+13.170	.04
DENSITY (N)			
Six Bands Median	.822	+15.280	.72
Bands 3, 4, 7 Median	.807	+17.992	.75
Standard Γ and $C_{r,2}$	.810	+7.887	.78
Hemisphere shape model	.807	+17.992	.75
Brightness and NDVI	.591	+36.750	.17

Table VII

AVERAGED REGIONAL ESTIMATES OF TREE SIZE ANDDENSITY

Region	n	R^2				N			
		Observed		Predicted		Observed		Predicted	
		mean	σ	mean	σ	mean	σ	mean	σ
Sudanian	6	23.16	7.30	27.42	10.24	26.10	13.69	38.22	25.80
Sahelian	8	9.65	3.23	12.89	5.25	130.57	38.83	123.97	44.40

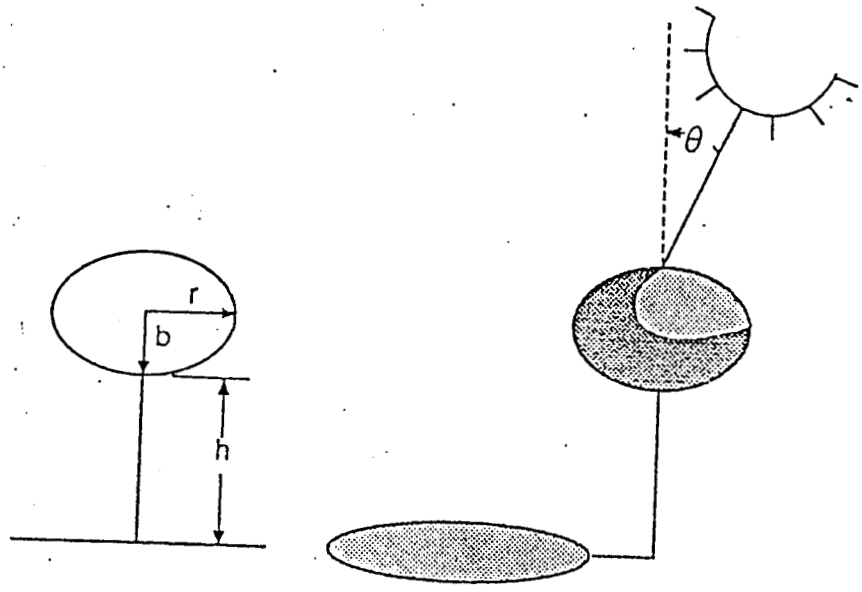

Fig. 1 — Tree shape and illumination geometry for an ellipsoid on a stick.

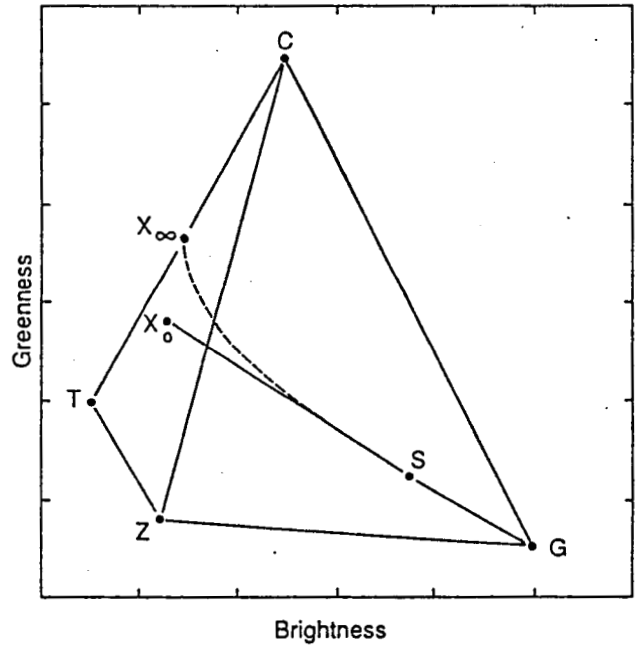

Fig. 2 — Idealized plot of spectral components on brightness and greenness spectral axes.

ORIGINAL PAGE IS
OF POOR QUALITY

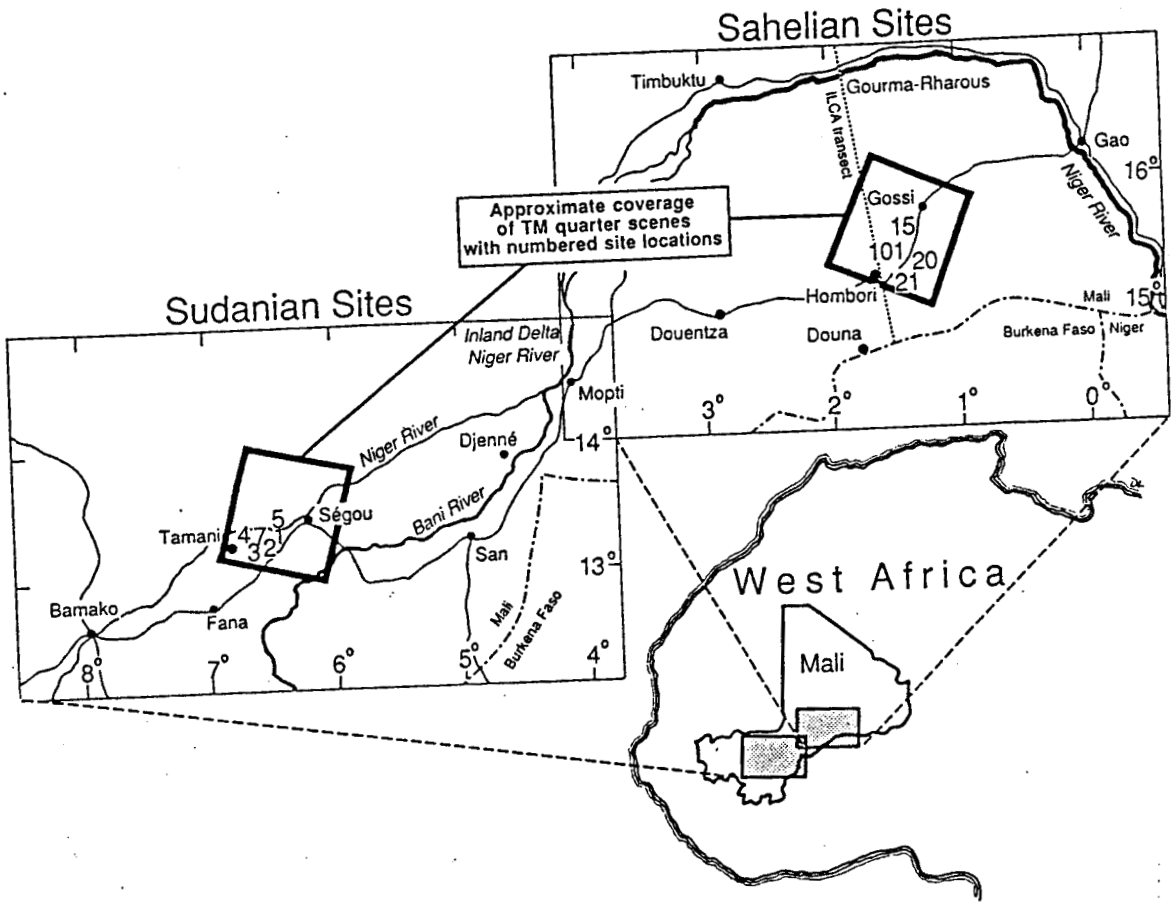

Fig. 3 — Location of test sites in West Africa.

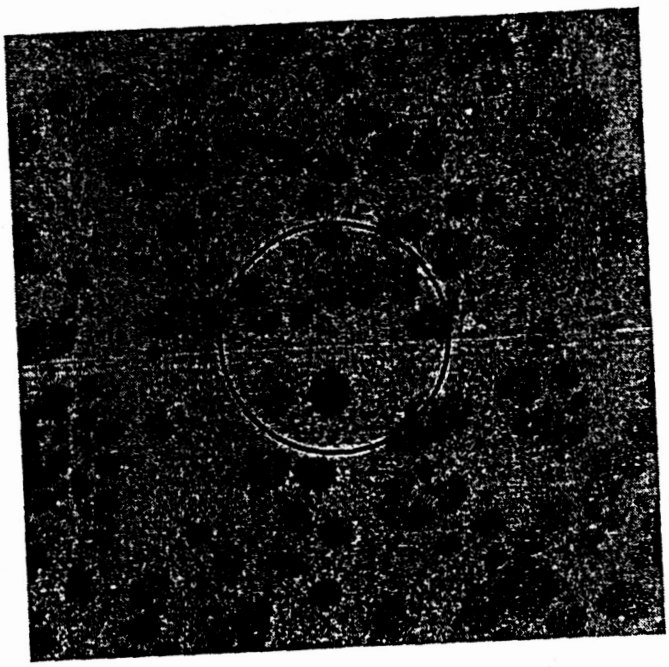

Fig. 4 — A portion of site 15 shown on an aerial photograph with plot size (25 m radius) indicated by the circle.

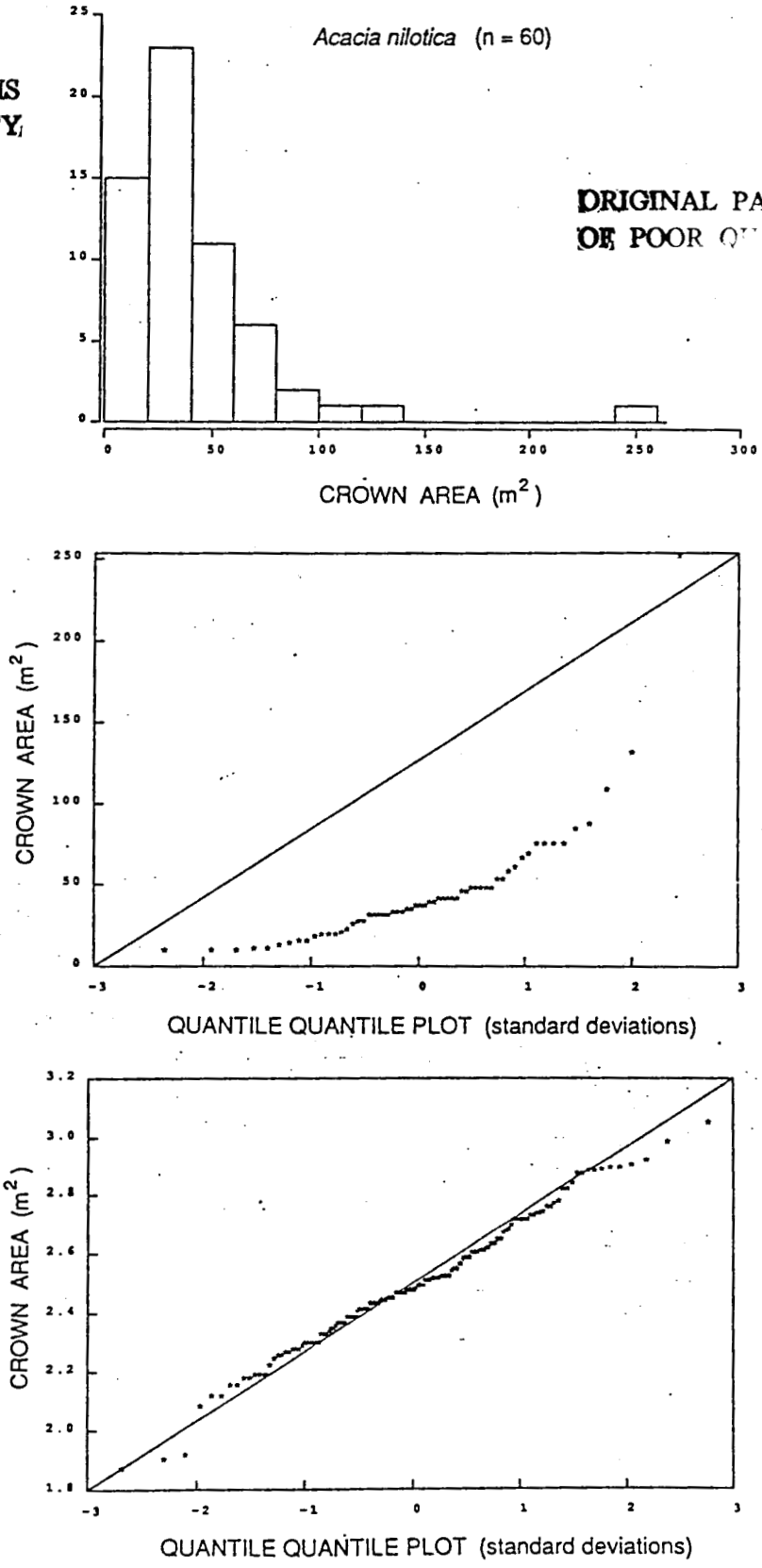

Fig. 5 — Histograms of size distributions for (a) *Acacia nilotica* (crown area) and (d) *Acacia albida* (height). The quantile-quantile (Q-Q) plots represent the data plotted against corresponding quantiles of the normal distribution (units are standard deviations). If the points fall in a straight line, they are normally distributed. (b), (e) raw values; (c), (f) lognormal values.

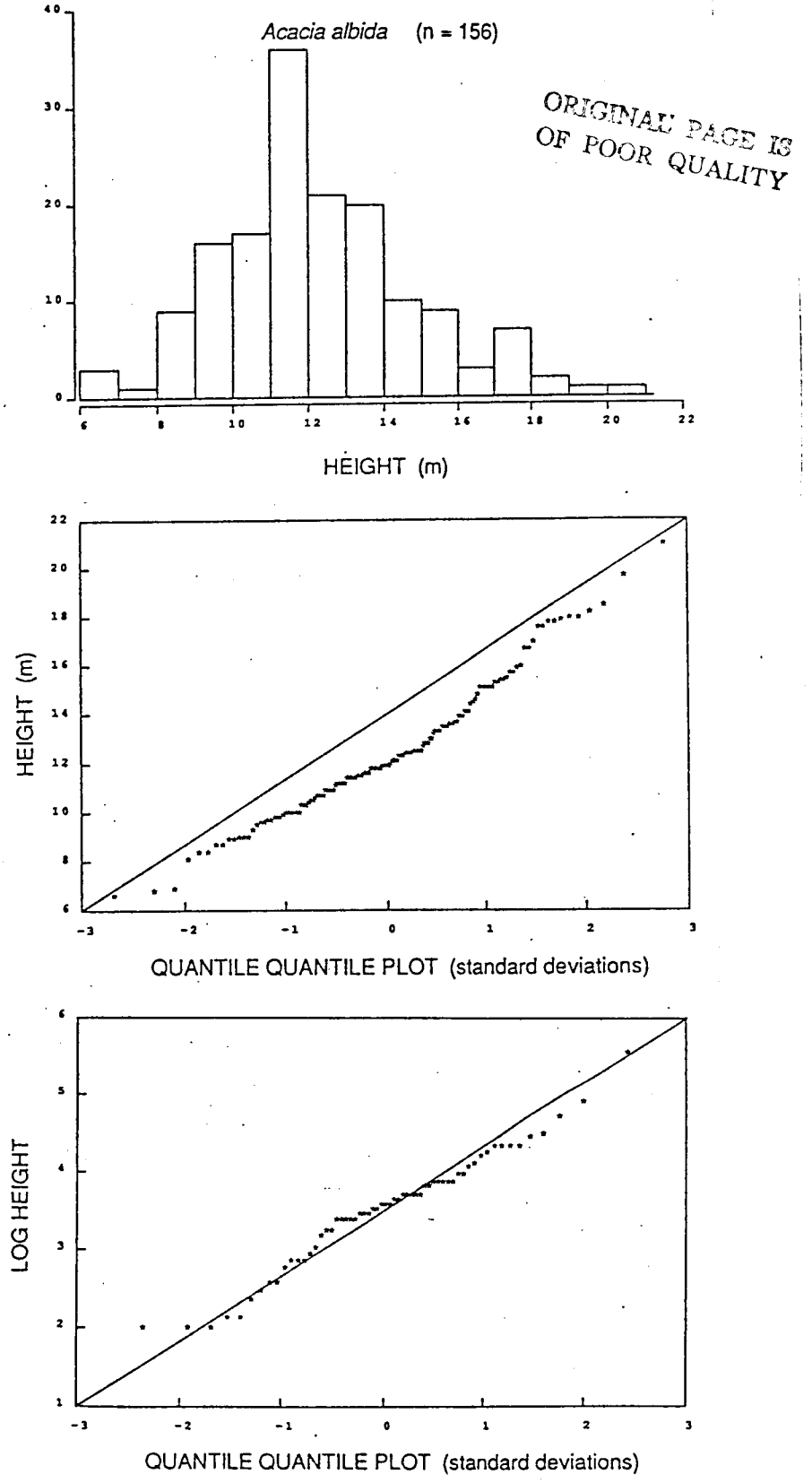

Fig. 5 — (cont.) Histograms of size distributions for (a) *Acacia nilotica* (crown area) and (d) *Acacia albida* (height). The quantile-quantile (Q-Q) plots represent the data plotted against corresponding quantiles of the normal distribution (units are standard deviations). If the points fall in a straight line, they are normally distributed. (b), (e) raw values; (c), (f) lognormal values.

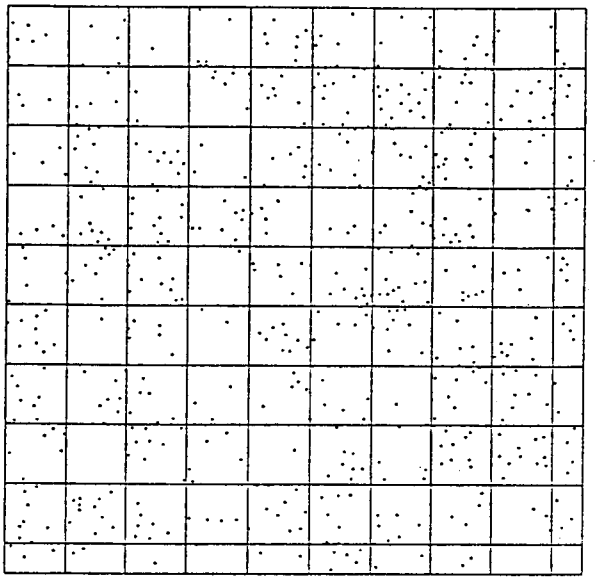

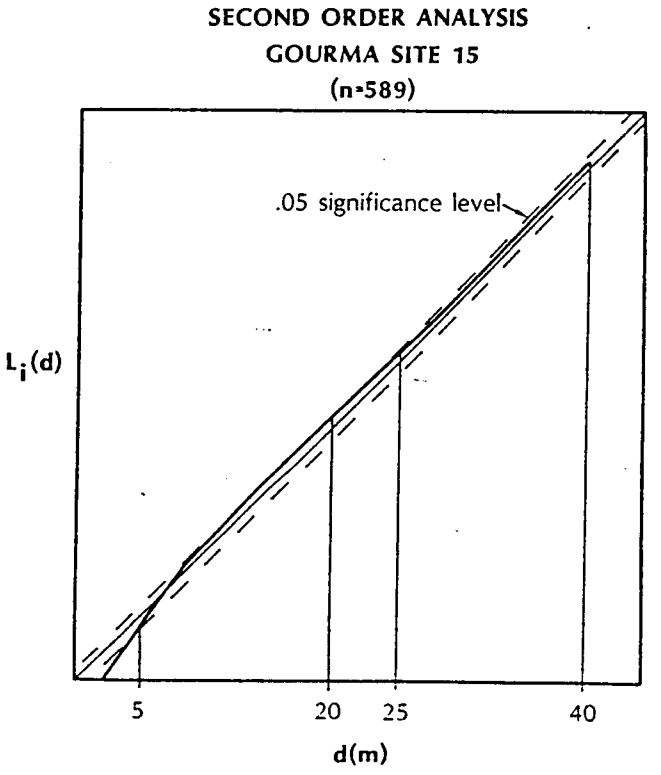

Fig. 6 — (a) Point locations of trees, Gourma Site 15 with grid of 30 m quadrats overlain. (b) Cumulative frequency of observed interpoint distances ($L_i[d]$). The diagonal is the expected frequency for a Poisson distribution, and the lines surrounding it are the .05 significance level.

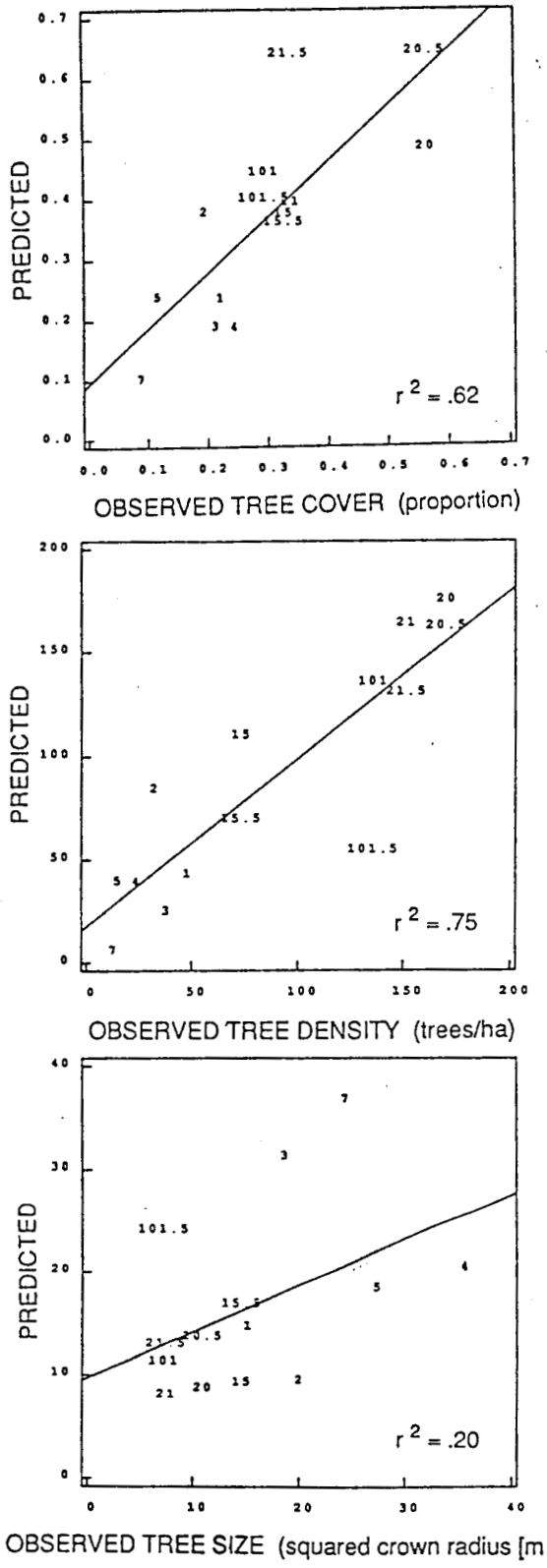

Fig. 7 — Observed vs. predicted stand parameters for Band 3, 4, 7 median, (a) cover, (b) density (N), (c) size (R^2), (d) cover substituting photointerpreted values for sites 2, 15, 20, (e) density with sample variance (± one standard deviation) and range of predicted values plotted, (f) size with sample variance (± one standard deviation), and range of predicted values plotted. A star (*) indicates predicted values in one band that is much greater than the range of the y-axis shown. Points are labeled by site number; numbers followed by .5 are based on 1985 TM data. All other points are based on 1984 spectral data.

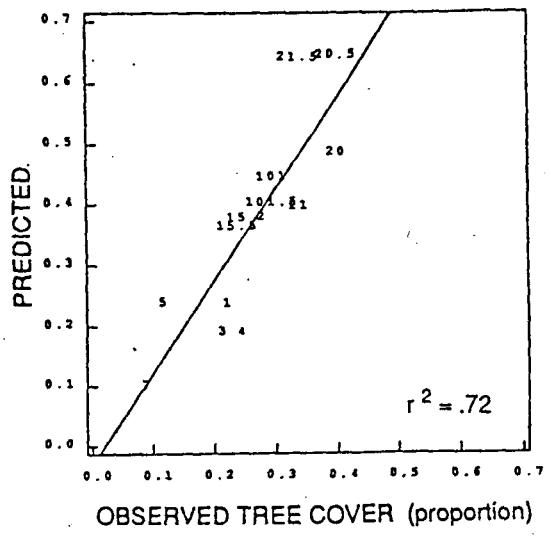

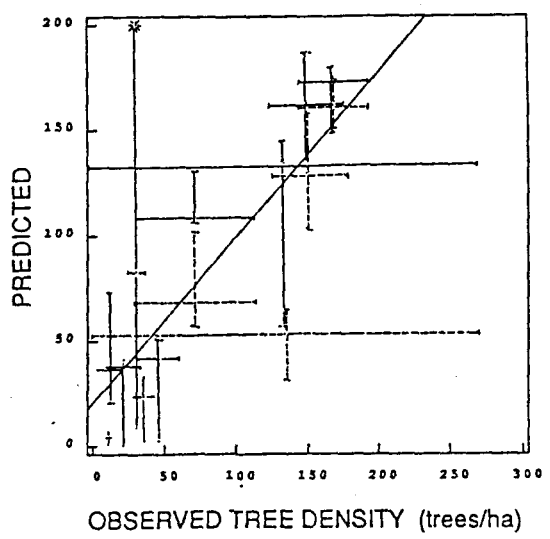

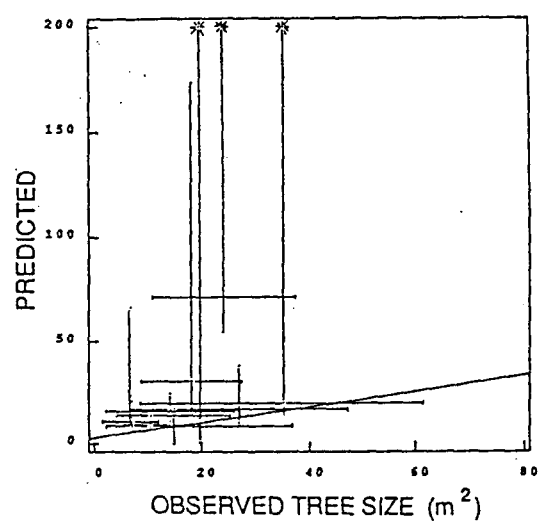

Fig. 7 — (cont.) Observed vs. predicted stand parameters for Band 3, 4, 7 median, (a) cover, (b) density (N), (c) size (R^2), (d) cover substituting photointerpreted values for sites 2, 15, 20, (e) density with sample variance (± one standard deviation) and range of predicted values plotted, (f) size with sample variance (± one standard deviation), and range of predicted values plotted. A star (*) indicates predicted values in one band that is much greater than the range of the y-axis shown. Points are labeled by site number; numbers followed by .5 are based on 1985 TM data. All other points are based on 1984 spectral data.

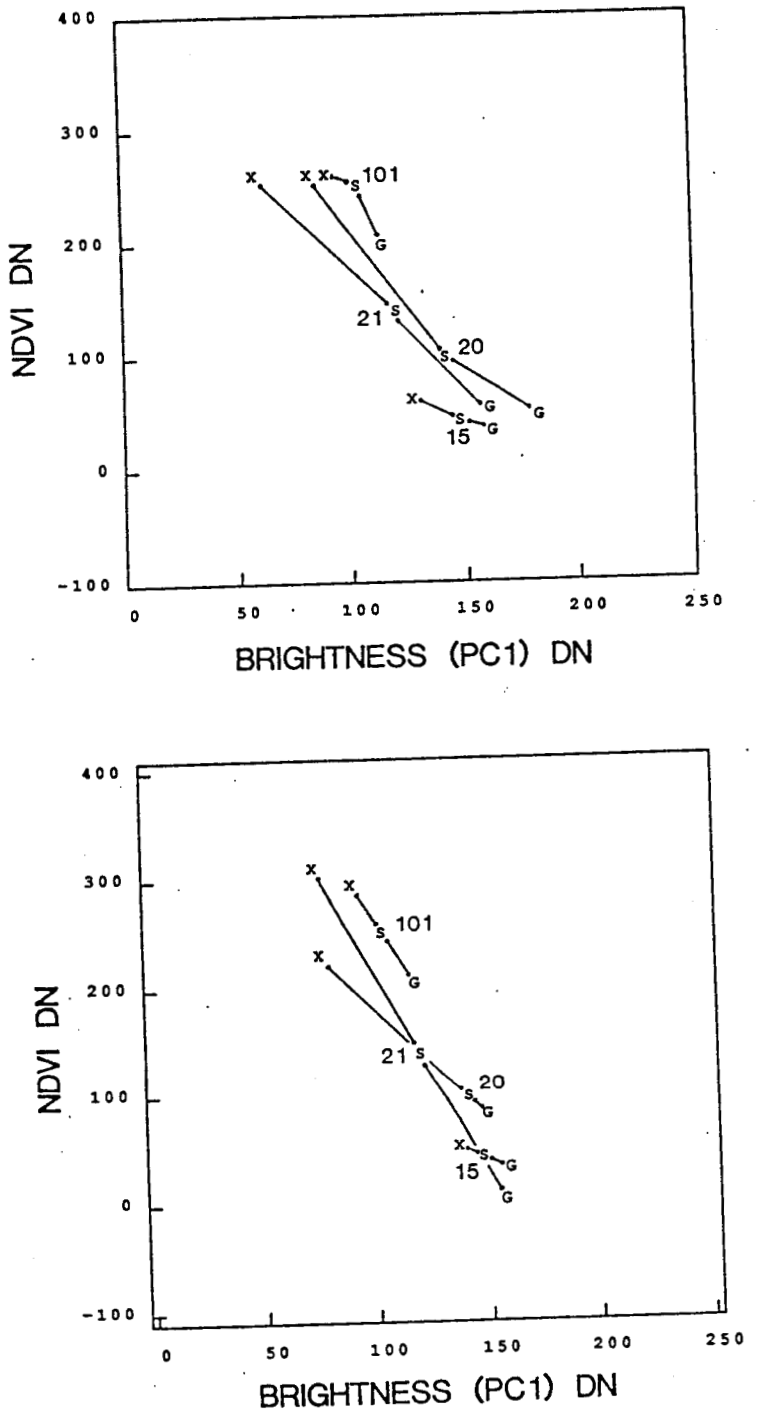

Fig. 8 — Component signatures for background (G), tree (X_0) and stand reflectance (S) plotted on brightness (PC1) and greenness (NDVI) transformed spectral axes, (a) observed G and X_0 and, (b) predicted G and X_0 for Sahelian sites, 1984 spectral data.

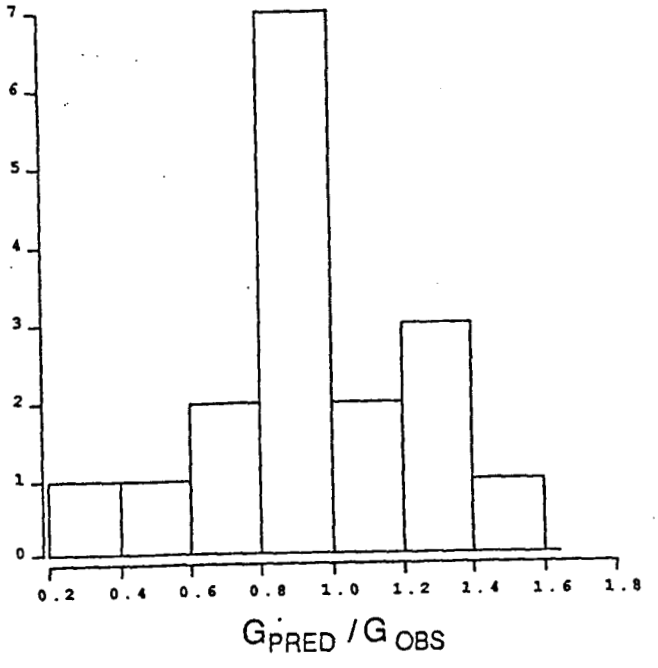

Fig. 9 — Histogram of G_{pred}/G_{obs} values for Sahelian sites, all TM Bands.

APPENDIX I.

WORK IN PROGRESS
SUPPORTED BY
NASA GRANT NGT-05-010-804

Estimating Leaf and Wood Biomass in Sahelian and Sudanian Woodlands Using a Remote Sensing Model

Janet Franklin

Department of Geography, University of California
Santa Barbara, California 93106, USA

and

Pierre H. Y. Hiernaux

International Livestock Centre for Africa
(Centre International pour l'Elevage en Afrique)
B. P. 60, Bamako, MALI, West Africa

Abstract

Predictions of tree size and density from a remote sensing model was used with allometric equations from the literature to estimate woody and foliage biomass in sparse woodland. Woodland sites were located in the Sudanian and Sahelian bioclimatic zones in Mali, West Africa, with cover ranging from ten to fifty percent. Our estimates are compared to independent measurements made in the Sahelian sites, and to typical values from the literature for these regions and for similar woodlands. If combined with a vegetation stratification at the appropriate scale, this approach could provide regional estimates of woody biomass for fuelwood inventory. Estimates of foliage biomass could be used in forage production modeling and inventory. Both could be used in regional and global scale models of biogeochemical cycling.

Reflectance properties of West African savanna trees from field radiometer measurements

JANET FRANKLIN AND DAVID S. SIMONETT
Department of Geography, University of California,
Santa Barbara, California 93106, U.S.A.
STEPHEN D. PRINCE[1] AND NIALL P. HANAN Present address: Earth Resources Branch (Code 623), NASA Goddard Space Flight Center, Greenbelt, MD, 20771, USA
School of Biological Sciences, Queen Mary College,
University of London, Mile End Road, London E1 4NS, England
ALAN H. STRAHLER
Department of Geology and Geography,
Hunter College of the City University of New York,
695 Park Ave, New York, New York 10021, U.S.A.

Abstract. Reflectance properties of savanna trees were measured using a pole-mounted radiometer for two Sahelian and two Sudanian species in West Africa. The measurements showed that canopy spectral components, viz shadowed and sunlit tree crown and background, have distinct reflectance characteristics in red and infrared wavebands as modelled by Li and Strahler (1986). Sunlit canopy is the greenest component, and sunlit background (consisting of bare soil) the brightest. Shadowed crown is the darkest component, and is greener than shadowed background. The field radiometer measurements were used to calculate the normalized difference vegetation index (NDVI), and the integrated NDVI over the canopy was related to leaf area and crown volume.

APPENDIX II.

PUBLICATIONS RESULTING FROM
WORK SUPPORTED BY
NASA GRANT NGT-05-010-804

CANOPY REFLECTANCE MODELING IN SAHELIAN AND SUDANIAN WOODLAND AND SAVANNAH

Janet Franklin

Department of Geography
University of California
Santa Barbara, CA 93106

Li Xiaowen
Alan H. Strahler

Department of Geology and Geography
Hunter College of the City University of New York
695 Park Ave, New York, New York 10021

ABSTRACT

A geometric-optical canopy reflectance model, driven by Landsat Thematic Mapper (TM) data, provided direct estimates of tree cover within twenty percent of actual values for several sparse woodland stands in West Africa. This model exploits tree geometry in an inversion technique to predict average tree size and density from reflectance data using a few simple parameters measured in the field (spatial pattern, shape, and size distribution of trees). Trees are treated as simply shaped objects, and multi-spectral reflectance of a pixel is a function of the proportion of tree crown, shadow, and understory in the pixel. These proportions are a direct function of the number and size of trees, and given the variance in reflectance within a homogeneous area of woodland, the model can be inverted to give estimates of average tree size and density. The model was tested in two sites in the Sahelian zone and five sites in the Sudanian zone, Mali. Tree density was consistently overestimated, and tree size underestimated, but correlation between observed and predicted values was very good ($r^2 > .85$). After improving our method for selecting component spectral signatures (for tree and background) results improved dramatically for stand estimates of tree size and density.

1. INTRODUCTION

A family of mathematical models of the reflectance of a plant canopy composed of discontinuous woody cover allows the direct estimation of plant size and density from remotely sensed reflectance data (Li and Strahler 1985). The models are geometric in character, treating trees (plants) as solid objects on a contrasting background, and estimating the proportion of each pixel in tree canopy, shadow, and background. In the simplest model, tree density is assumed to be low, and trees and shadows do not overlap enought to change the proportion of shadow in a pixel. Using this simple model, Li and Strahler (1985; Strahler and Li 1981) predicted tree size and density within ten percent of actual values for sparse pine forest in northern California from Landsat MSS data.

We have extended this model and tested it using Landsat Thematic Mapper (TM) data in a new environment where the basic assumptions of the model hold, but the parameters must be modified. The model was tested in sparse woodland and wooded grassland in the Sahelian and Sudanian bioclimatic zones in West Africa. Dry woodlands and wooded grasslands are important ecologically and economically in Africa, and cover forty percent of the continent by some estimates. The depletion of woody cover due to changes in land use practices, coupled with increasing population and

*Presented at the Twentieth International Symposium on Remote Sensing of Environment, Nairobi, Kenya, 4-10 December 1986

drought, is a severe problem for people living in these areas where trees are used for fuel and fodder.

Our method can be used as part of a multi-stage inventory to directly estimate the size and density of woody plants over large areas. Because size and spacing are often related to leaf and woody biomass, this technique could also provide woodland biomass estimates over large areas.

Further, an important application of global remote sensing is the estimation of ecosystem productivity using spectral greenness measures from the AVHRR sensor (Justice et al. 1985, Tucker et al. 1985a, Tucker et al. 1985b). One problem with this approach is that the relationship between the spectral index and green biomass is affected by woody cover (and other factors such as soil background and atmosphere; Hiernaux and Justice 1986, Holben and Fraser 1984). Our model could help improve these methods by providing tree density estimates within vegetation strata, for adjusting the greenness index/biomass relationship.

2. BACKGROUND

Plant canopy modeling provides a way of understanding the reflectance of a vegetated surface by building a functional model of reflectance based on the biophysical, optical, and spatial properties of the scene elements (plants or plant parts). If a reflectance model can be *inverted* the biophysical properties of the plant stand can be inferred from spectral reflectance measurements. The simple Li-Strahler model uses covariance statistics from estimated mixtures of scene components across pixels for inversion, to predict average tree size and density in a stand. This model is discussed in great detail in Li and Strahler (1985) and Li (1983) and will only be described briefly here. The assumptions of the model are as follows:

— a tree crown is a simple geometric form, in this case a hemisphere on a stick (Fig. 1).

— tree counts vary from pixel to pixel as a Poisson function with a fixed density (e. g. — the spatial pattern is random at the scale of sensor resolution)

— the size distribution function of trees is known, so that C_{R^2}, the coefficient of variation of squared crown radius, can be determined for the stand.

— the tree crown and its associated shadow have a spectral signature which is distinct from that of the understory (background).

The reflectance of a pixel is modeled as a linear combination of the signatures of scene components (tree crown, background, shadowed tree and background) weighted by their relative areas. Pixels from an area of homogeneous tree cover can be taken as replicate measures of reflectance. Interpixel variance comes from variance in the number of trees among pixels and variation in the size of trees within and between pixels (if chance overlapping of trees and shadows is ignored).

From the reflectance values the parameter m ($= NR^2$) can be calculated, where N is the average tree density, and R^2 the average squared crown radius. Note that $m\,\pi$ is equal to the proportion of woody cover in the stand. If N and R^2 are uncorrelated (a reasonable assumption is a sparse stand) then the expression for mean and variance of two independent products will apply, and mean size and density can be separated using the mean and variance of stand reflectance.

The model also includes a geometric factor, Γ, which is defined such that $m\,\Gamma$ is the proportion of a pixel covered by tree crown and shadow. Γ can be calculated from the tree-shape geometry and the sun angle. The reflectance signatures of the model are:

G Reflectance vector for a unit area of illuminated background (constant).

C Reflectance of a unit area of illuminated crown (constant).

Z Reflectance of a unit area of shadowed background (constant).

T Reflectance of a unit area of shadowed crown (constant).

S Reflectance of a pixel. Variable; depends on number and size of trees in pixel.

$V(S)$ Variance in reflectance of all pixels in a stand.

The signature of pixel i in band j is then modeled as

$$S_{ij} = G_j \cdot K_g + (1-K_g)\cdot(C_j \cdot K_c + Z_j \cdot K_z + T_j \cdot K_t)\,. \qquad (1)$$

where

K_g Proportion of pixel not covered by crown or shadow.

K_c Proportion of area covered by crown and shadow that is in illuminated crown.

K_t Proportion of covered area in shadowed crown.

K_z Proportion of covered area in shadowed background.

Because K_c, K_z, and K_t sum to one (by definition), the expression $(C_j \cdot K_c + Z_j \cdot K_z + T_j \cdot K_t)$ represents a point in multispectral space lying within a triangle with vertices at C, Z, and T (see Figure 1). This point is X_0; the average reflectance of a tree and its associated shadow. When m varies, S will vary along a straight line connecting points G and X_0.

The area of a pixel which is not background $(1 - K_g)$ was previously defined as $m\Gamma$. So, $K_g = 1 - m\Gamma$. Therefore, dropping the subscripts, (1) can be written

$$S = G(1 - m\Gamma) + X_0 m\Gamma$$

and rearranging, we have

$$m = \frac{G - S}{\Gamma(G - X_0)} . \tag{2}$$

From (2) we can derive the variance of m:

$$V(m) = \frac{V(S)}{\Gamma[(G - X_0)]^2} . \tag{3}$$

In the multiband case, m should be the same if determined from any band. However, variance in the signatures and stand parameters will cause m to vary, and thus m can be taken as a weighted average. Because $(G - X_0)$ is in the denominator, sensitivity to variance and noise in S, G and X_0 will be reduced when spectral contrast between trees and background is high.

If size and density are independent, then the mean and variance of m are the mean and variance of independent products, and the following expressions apply:

$$M = E(nR^2) = E(n) \cdot E(R^2) = N\mathrm{R}^2 , \tag{4}$$

and

$$V(m) = V(nR^2) = (\mathrm{R}^2)^2 V(n) + N^2 V(R^2) + V(n)V(R^2) . \tag{5}$$

Because n is a Poisson function,

$$V(n) = N . \tag{6}$$

Further,

$$V(R^2) = V(r^2)/n \approx V(r^2)/N = C_{R^2}(E(r^2))^2/N \tag{7}$$

because $C_{R^2} = V(r^2)/(E(r^2))^2$. Substituting (6) and (7) into (5),

$$V(m) \approx (N + C_{R^2} N + C_{R^2})(\mathrm{R}^2)^2 = (M + C_{R^2} M + C_{R^2} \mathrm{R}^2)\mathrm{R}^2 . \tag{8}$$

Solving for R^2, we obtain:

$$\mathrm{R}^2 = \frac{[(1 + C_{R^2})^2 M^2 + 4V(m)C_{R^2}]^{1/2} - (1 + C_{R^2})M}{2C_{R^2}} . \tag{9}$$

Applying the approximation $\sqrt{1 + x} \approx 1 + x/2$, we obtain

$$\mathrm{R}^2 = \frac{V(m)}{(1 + C_{R^2})M} . \tag{10}$$

3.

Finally, substituting (2) and (3), the expressions for mean and variance of m, into (10), R^2 can be found from the reflectance values of a pixel in a stand, and the N can be found using (4).

3. STUDY SITES IN MALI

Sahelian test sites in the Gourma region of Mali were chosen from among those being monitored by ILCA/Mali (The International Livestock Centre for Africa) in collaboration with the GIMMS Project (Global Inventory, Monitoring and Modeling System; National Aeronautics and Space Administration, Goddard Space Flight Center). Two sites were used for the initial test of the model, ILCA Sites 15 and 20. Site 15 is located in an *Acacia nilotica* woodland (approximately 31 percent cover), on an alluvial plain of poorly drained vertisols. Site 20 is located in an *Acacia seyal* woodland (approximately 58 percent cover), also on an alluvial plain of vertisols that is inundated during the rainy season, but more freely drained that Site 15 (Hiernaux *et al.* 1984).

The Sudanian test sites are located in the Region of Ségou. The crop/woodland type of vegetation is formed when crops are grown under a woodland of useful trees which are preserved when land is cleared. Sites 1 and 2 are dominated by *Vitellaria paradoxa* (called shea, karité, or shi), and Sites 3, 4N and 4S are dominated by *Acacia albida* (balanzan). All sites are located in the house fields (cultivated areas near the village where shrubs and weeds are cleared regularly) and cover range from 13 to 25 percent.

4. METHODS

A hemispherical shape was initially chosen to test the model in savanna, based on field reconnaissance. Tree height (H) and crown diameter (= $2r$) were measured for thirty to one hundred trees in each site, and average h (see Fig. 1) was calculated from $H - R$ for the stand. The ratio h/R was used to calculate Γ from the geometry of the hemisphere. Size distribution was examined by inspecting histograms of tree size (expressed both as crown size and height) for all sites. The model parameter C_{R^2} was calculated from sample data for the sites. Spatial pattern was established by mapping point patterns of 200-900 trees from low-altitude aerial photographs in sample quadrats within the test sites, and analyzing using quadrat analysis (Li and Strahler 1981, Franklin et al. 1985), and second-order analysis of inter-tree distances (Franklin and Getis 1985).

Landsat Thematic Mapper (TM) data were used to test this model. Early dry season imagery was chosen to enhance the contrast between trees (still green for most species) and understory (a dry herbaceous layer, or bare soil). The TM scene for the Gourma sites was acquired 9 September 1984 at the end of a very bad growing season in the Sahel. The scene for the Ségou sites dates from 17 November 1984, after the harvest, so the fields beneath the canopy have been cleared. The mean and variance of reflectance (S and $V(S)$) were computed for each of the test sites. Signatures for background and canopy (G and X_0) were computed from small training areas in the image, using aerial photographs as a guide. Areas of no tree cover in or near sites were used to estimate G, and pixels with high tree cover were used to estimate X_0.

The model was tested by inputting the stand parameters (Γ and C_{R^2}) and the spectral parameters (G, X_0, S and $V(S)$), predicting R^2 and N for each site, and comparing to actual R^2 and N from field measurements. Observed and predicted values were compared by simple regression. The model was tested using TM Bands 3 (.63-.69 μm) and 7 (2.08-2.35 μm). Band 3 was chosen because in our experience red reflectance is strongly related to tree cover (Logan and Strahler 1982, Franklin 1986), and Band 7 had the highest variance in the sites, and has also been shown to be related to tree cover (Horler and Ahern 1986).

5. RESULTS

Table I shows the stand parameters h/R, R, C_{R^2} and Γ for all sites. Values for H/R range from 1 to 1.6 for Ségou sites (taller trees, narrower crowns) and 0.5 to 0.6 for Gourma sites (shorter trees, wider crowns). C_{R^2} values range from 0.21 to 0.69.

Tree size distributions for all sample populations were slightly to extremely right-skewed, and a log-transform produced a normal-looking distribution (Fig. 3). Thus, if field measurements were not available, the assumption of a lognormal size distribution is supported for these sites, and the formula for C_{R^2} for a lognormal distribution could be used. However, for these sites C_{R^2} was calculated directly from sample data.

Table I. Stand Parameters

Site	Species	n	h/R	R	C_{R^2}	Γ
15	*A. nilotica(*)*	56	.50	3.63	.6850	4.37
20	*A. seyal(*)*	87	.62	3.23	.4401	4.55
1	*V. paradoxa*	33	1.22	3.62	.6166	6.73
2	*V. paradoxa*	32	1.06	3.88	.2560	6.44
3	*A. albida*	32	1.50	4.44	.2672	7.11
4N	*A. albida*	14	1.17	6.57	.2125	6.63
4S	*A. albida*	16	1.64	4.66	.3816	7.19

Fig. 4 shows the point locations and results of second order analysis for one of the sites. In all sites there is generally an inhibition distance of five to ten meters, below which the probability of finding two trees is very low, but at relevant sensor resolution (20 to 50 m) a Poisson model is adequate. This is supported by the quadrat analysis. At larger distances (50 to 100 m) a Poisson model still fits in many of the sites, including the sparser stands (Site 2) at densities where the Poisson model broke down in our earlier studies (Franklin et al. 1985).

The results of the model test are shown in Table II which includes the model parameters and observed and predicted values values of R^2 and N. The model consistently overestimates density and underestimates crown size, but predicted cover values are very close to actual cover based on field measurements, and there is good correlation between observed and predicted values of N and R^2 (Table IV). Table III shows the rank order of observed and predicted R^2, N and Cover for TM Bands 3 and 7. Rank order is preserved in most cases. The model easily separates big crown, low density stands from large crown, high density stands.

Table II. Results Canopy Model Inversion TM Band 3 (.63–.69μm)

Site	G_{ob}	G_{pr}	X_{0ob}	X_{0pr}	S	$V(S)$	Area(ha)	$R^2_{ob}(m^2)$	R^2_{pr}	$No\,(/pix)$	N_{pr}	C_{ob}	C_{pr}	%
15	149.9	137.6	108.5	108.2	124.7	43.4	71.6	14.04	5.04	6.42	24.66	.31	.44	70
20	151.9	141.0	102.2	114.8	119.1	44.4	72.0	10.62	3.78	15.57	34.92	.58	.46	79
1	103.1	102.4	68.7	72.1	90.7	59.4	51.8	13.86	11.43	3.73	4.22	.18	.17	94
2	98.2	95.4	68.7	58.1	84.8	56.9	92.5	16.02	16.02	2.48	3.97	.14	.22	64
3	98.2	96.9	79.0	77.0	86.7	37.1	86.2	18.18	16.74	3.58	4.52	.23	.26	88
4N	110.5	106.4	83.0	86.8	95.9	83.3	25.2	45.63	23.13	1.59	3.28	.25	.26	96
4S	108.6	104.0	83.0	86.4	98.7	24.6	18.1	24.21	8.82	1.55	5.50	.13	.17	76
Using X_0 and G from 4N,								predict R^2 and N						
4S	106.4		86.8		98.7	24.6		24.21	14.76	1.55	3.33	.17	.17	100

Table III. Rank Order of Predicted and Observed Size, Density and Cover

Band 3		Band 7		Band 3		Band 7		Band 3		Band 7	
R^2				N				*Cover*			
Pred	Obs	Pred	Obs	Pred	Obs	Pred	Obs	Pred	Obs	Pred	Obs
20	20	20	20	4N	4S	2	4S	4S	4S	4S	4S
15	1	15	1	2	4N	4S	4N	1	2	2	2
4S	15	1	15	1	2	4N	2	2	1	1	1
1	2	4S	2	3	3	3	3	3	3	3	3
2	3	3	3	4S	1	1	1	4N	4N	4N	4N
3	4S	4N	4S	15	15	15	15	15	15	15	15
4N	4N	2	4N	20	20	20	20	20	20	20	20

We noted that it is difficult to accurately characterize component signatures using training data. Using our training technique, the observed G was too bright, and observed X_0 too dark in most cases. Overestimating G caused the individual predictions of N to be too high, and R^2 too low. Therefore, our next approach was to predict the component signatures (G and X_0) using the model, based on observed N and R^2 for the sites. Table II shows predicted values of G and X_0. In all cases there is a good correlation between observed and predicted spectral variables (G and X_0); see Table IV. To see if signature extension is possible, predicted values of G and X_0 from Site 4N were used to predict N and R^2 in Site 4S (same type of woodland, different size and density). The bottom entry in Table II show that the predicted values match observed more closely when component signatures are predicted from the model, and then extended in this way.

Table IV. Regression Equations and r^2 for Observed and Predicted Values

Variable	Band	Regression Equation	r^2
R^2	3	$Obs = 1.279(Pred) + 5.013$	.56
	7	$Obs = 1.781(Pred) - 0.560$	.68
N	3	$Obs = 0.358(Pred) + 0.835$	.86
	7	$Obs = 0.459(Pred) + 0.625$	.95
Cover	3	$Obs = 1.117(Pred) + 0.056$	.75
	7	$Obs = 1.033(Pred) + 0.309$	.75
G	3	$Obs = 0.741(Pred) + 20.396$	.88
X_0	3	$Obs = 1.251(Pred) + 23.330$	.99

We also ran the model holding the stand parameters h/R and C_{R^2} constant for all stands (we chose intermediate values from among those measured in the field) and predicted R^2 and N, to test the sensitivity of the model to these parameters. Table V shows the results for constant values of h/R and C_{R^2}. There is little change in the predicted values of R^2 and N, no systematic error caused by holding the stand variables constant, and no change in the rank order of observed and predicted values.

Table V. Model Results for Constant h/R (=1) and C_{R^2}(=.5)
(Band 3; G, X_0, S, and $V(S)$ same as in Table 3)

Site	R^2_{obs}	R^2_{pred}	N_{obs}	N_{pred}	C_{obs}	C_{pred}	%
15	14.04	4.86	6.42	21.95	.31	.37	84
20	10.62	3.15	15.57	36.35	.58	.40	69
1	13.86	13.14	3.73	3.91	.18	.18	100
2	16.02	13.59	2.48	4.74	.14	.22	64
3	18.18	15.93	3.58	5.35	.23	.30	77
4N	45.63	19.63	1.59	3.84	.25	.26	96
4S	24.21	9.18	1.55	5.98	.13	.19	68

6. DISCUSSION

Using the Li-Strahler simple variance-dependent canopy model, characterizing tree geometry, spatial and size distribution from field data, and deriving spectral data from TM imagery, we were able to predict tree cover in test sites with reasonable accuracy (80 to 100 percent using TM Band 7, 60 to 100 percent using TM Band 3). The model easily separates low from high density stands; rank order of observed and predicted cover values are similar.

The model is relatively insensitive to the stand parameters Γ (which predicts the amount of tree crown and associated shadow from the geometry of the trees), and C_{R^2} (the variance in tree size) as shown by the results using a standard value for h/R (from which Γ is calculated) and C_{R^2}. This mean that reasonable values for h/R and C_{R^2} can be chosen for a species or woodland type, and extended over large areas.

In this test, the model underestimates crown size and overestimates density in all sites. The correlations between observed and predicted values shows that density is predicted better that crown size. The problem appears to be that our technique for choosing component signatures overestimates the brightness of G, to which the model is very sensitive, and in most cases underestimates the brightness of X_0. However, regressions of observed and predicted G and X_0 values show very good correlation ($r^2>.85$), so it may be possible to adjust values of G and X_0 from training data by simple regression. Another alternative is to predict G and X_0 using the model itself in test sites where size and density are known, and then extrapolate these signatures to other areas. This was tested in Sites 4N and 4S, with greatly improved predicted values of N and R^2.

7. CONCLUSIONS

The Li-Strahler canopy model provides a physically-based model which explains the major characteristics of reflectance, and variance in reflectance, in a sparsely wooded landscape in terms of variations in tree size and density, and shadowing geometry. This gives a functional explanation for the observed empirical relationship between reflectance (brightness) and tree cover.

As a technique, this model is most useful when it can be parameterized and run over large areas. Therefore, it needs to be tested further in the following ways. Sites need to be divided into "train" and "test" portions, to see if signature and parameter extension is possible. More sites, over a greater range of crown size and density, need to be included. The accuracy of predicted N and R^2 should be improved by averaging predictions from uncorrelated spectral bands, principal components, or multi-date imagery, and this must be tested. Further, this technique is most cost-effective when applied to the coarsest spatial resolution for which inter-pixel variance is sufficient to invert the model. This can be tested with lower resolution imagery, or by resampling TM to simulate lower resolution imagery. Finally, our field work this year has convinced us that an ellipsoid is a better shape model than a hemisphere in this landscape, and in future work, Γ will be calculated accordingly.

8. ACKNOWLEDGEMENTS

This work would not have been possible without the scientific and logistic support of Pierre Hiernaux and the personnel at ILCA/Mali, and Chris Justice and the GIMMS personnel, research authorization from the Ministère Education National, Mali, and the cooperation of the people in our study zones. We thank David Simonett, Dramane Dembélé, Dramane Diarra, Roy Cole and Moussa Traoré for field assistance. This work was supported by the National Aeronautics and Space Administration (NASA), Awards NAGW-788 and NGT 05010804.

9. REFERENCES

Franklin, J., "Thematic Mapper analysis of coniferous forest structure and composition," *International Journal Remote Sensing*, vol. 7, pp. 1287-1301, 1986.

Franklin, J. and A. Getis, "A second order analysis of the spatial pattern of Ponderosa pine," *American Association for the Advancement of Science, annual meeting*, Los Angeles, California, 1985.

Franklin, J., J. Michaelsen, and A. H. Strahler, "Spatial analysis of density dependent pattern in coniferous forest stands," *Vegetatio*, vol. 64, pp. 29-36, 1985.

Hiernaux, P., M. I. Cissé, and L. Diarra, "Bilan d'une saison d'es pluies 1984 tres deficitaire dans la Gourma (Sahel Malien). Première campagne de suivi et télédetection expérimentale, Annexe: Fiches descriptives des sites," Programme des Zones Aride et Semi-aride, Document du Programme, CIPEA, Bamako, Mali, 1984.

Hiernaux, P. and C. O. Justice, "Suivi du developpement vegetal au cours de l'ete 1984 dans le Sahel Malien," *International Journal of Remote Sensing*, 1986. In press.

Holben, B. N. and R. S. Fraser, "Effects of atmosphere and view illumination geometry on visible and near IR AVHRR radiance data," *International Journal of Remote Sensing*, vol. 5, pp. 145-160, 1984.

Horler, D. N. H. and F. J. Ahern, "Forestry information content of Thematic Mapper data," *International Journal of Remote Sensing*, vol. 7, pp. 405-428, 1986.

Justice, C. O., J. R. G. Townshend, B. N .Holben, and C. J .Tucker, "Analysis of the phenology of global vegetation using meteorological satellite data," *International Journal of Remote Sensing*, vol. 6, pp. 1271-1318, 1985.

Li, X., "Geometric-optical modeling of a conifer forest canopy," Ph.D. Dissertation, Department of Geography, University of California, Santa Barbara, CA, 1983.

Li, X. and A. H. Strahler, "Geometric-optical modeling of a conifer forest canopy," *IEEE Transactions on Geoscience and Remote Sensing*, vol. GE-23, pp. 705-721, 1985.

Logan, T. L. and A. H. Strahler, "Optimal Landsat transforms for forest applications," *Proceedings of the 16th International Symposium on Remote Sensing of Environment*, pp. 455-468, Ann Arbor, Michigan, 1982.

Strahler, A. H. and X. Li, "An invertible forest canopy reflectance model," *Proceedings of the Fifteenth International Symposium on Remote Sensing of Environment*, Environmental Research Institute of Michigan, Ann Arbor, 1981.

Tucker, C. J., J. R. G. Townshend, and T. E Goff, "African land-cover classification using satellite data," *Science*, vol. 277, pp. 369-375, 1985.

Tucker, C. J., C. Vanpraet, E. Boerwinkel, and A Gaston, "Satellite remote sensing of total dry matter production in the Senegalese Sahel," *Remote Sensing of Environment*, vol. 13, pp. 461-474, 1985.

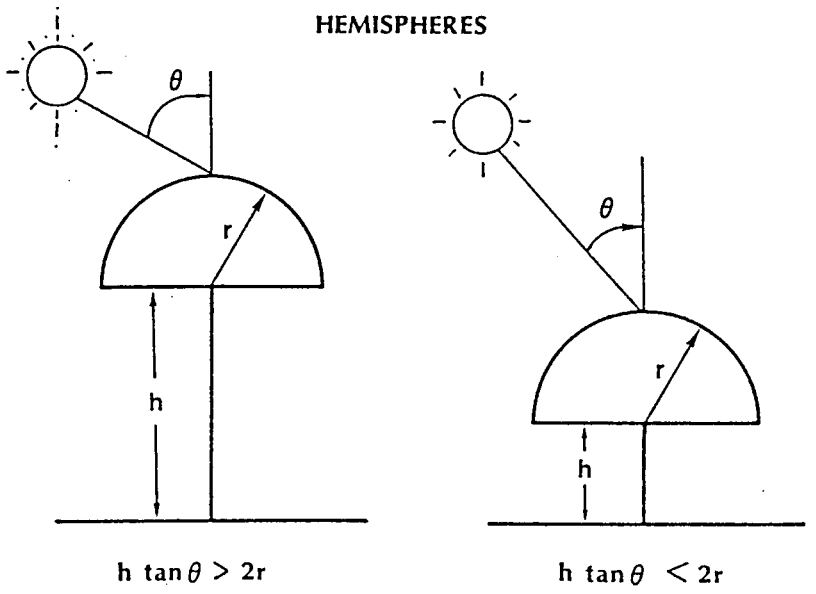

Figure 1. Tree form geometry.

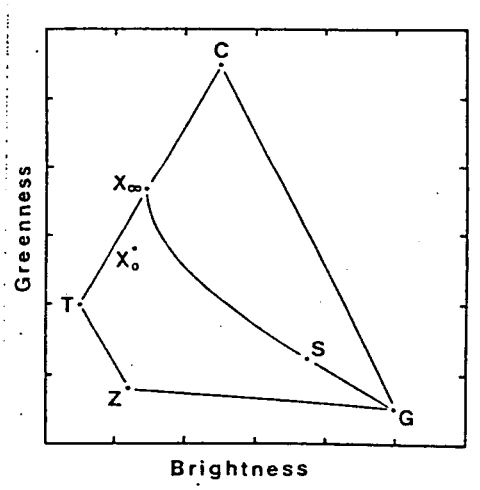

Figure 2. Idealized plot of model in multispectral space.

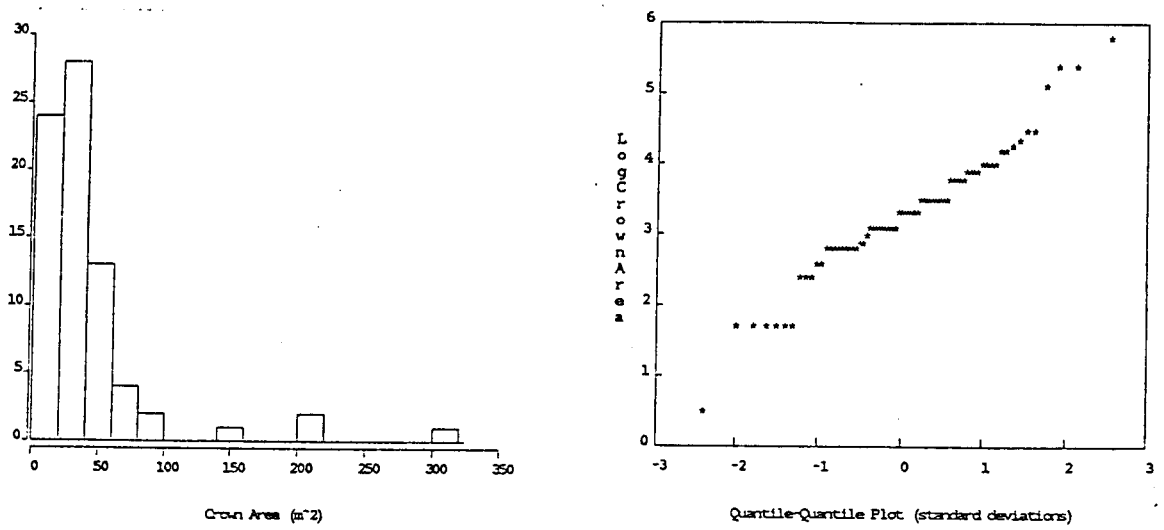

Figure 3. Size distribution of trees and Q-Q plot of log transform for Site 15.

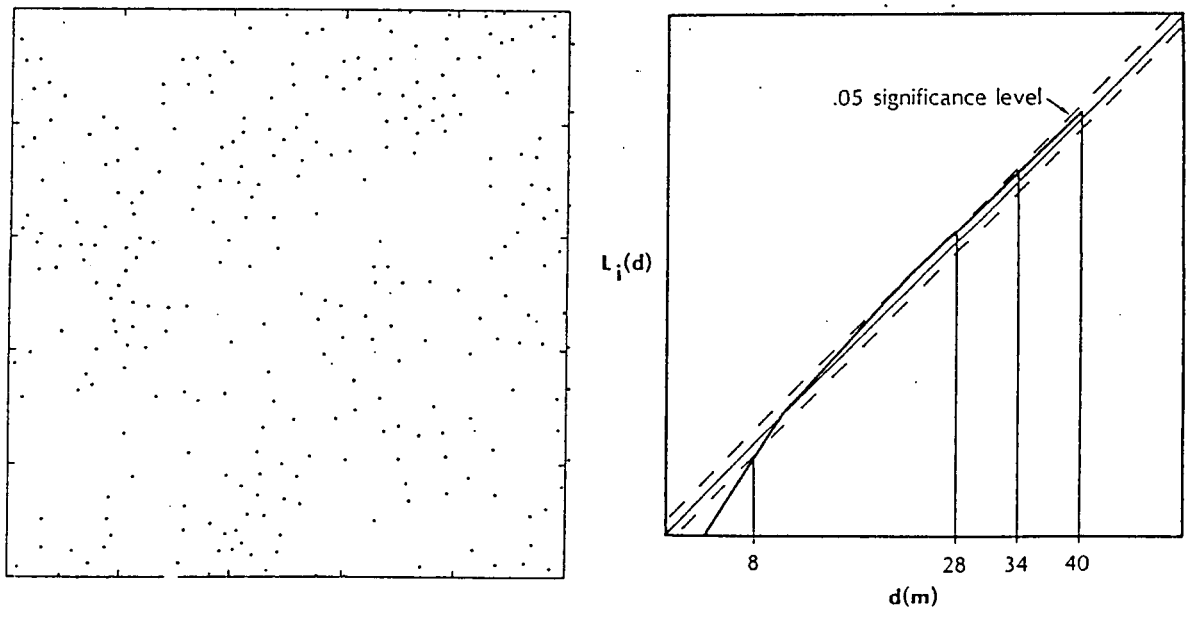

Figure 4. Point locations and results of second order analysis for Site 2.